AD NUMBER

AD462729

NEW LIMITATION CHANGE

TO

Approved for public release, distribution unlimited

FROM

Distribution authorized to U.S. Gov't. agencies and their contractors; Administrative/Operational Use; JAN 1965. Other requests shall be referred to Office of Naval Research, 875 North Randolph Street, Arlington, VA 22203.

AUTHORITY

ONR ltr dtd 4 May 1977

UNCLASSIFIED

DEFENSE DOCUMENTATION CENTER

FOR

SCIENTIFIC AND TECHNICAL INFORMATION

CAMERON STATION ALEXANDRIA. VIRGINIA

MC-61-5-R

NEAR FIELD INFRARED
BACKGROUND NOISE SIMULATION

BY

RICHARD H. ADAMS

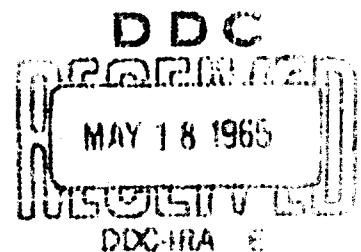INTERIM ENGINEERING REPORT

JANUARY 1965

MITHRAS, Inc.

AEROTHERMODYNAMICS - ELECTROMAGNETICS - QUANTUM

701 CONCORD AVENUE

MC 61-5-R5

NEAR FIELD INFRARED
BACKGROUND NOISE SIMULATION

by

Richard H. Adams

Interim Engineering Report

Nonr Contract 3489(00)

January 1965

FOREWORD

This report was prepared by MITHRAS, Inc., for the Department of the Navy's Office of Naval Research and Bureau of Naval Weapons under Contract Nonr 3489(00). Scientific officers for ONR Air Programs have been Lt. Cmdr. S. D. Kearney and Cmdr. M. Gussow, and for BuWeps Missile Division, J. M. Lee.

The research reported here was begun in February 1964 and completed in October 1964. It was essentially a continuation of research performed under Contract Nonr 3733(00).

ABSTRACT

Studies on the near field infrared background noise problem have been directed towards the simulation of the infrared noise emanating from a known turbulent zone. A laboratory tool for simulating the near field noise has been designed, utilizing a simple heated round free subsonic jet as the infrared noise generator. A review of the characteristics of the hot free subsonic jet is presented and the design of the near field infrared background simulator is described. Preliminary measurements of the fluctuations in radiant emittance from the jet have been made with an AC radiometer. The data have been reduced to normalized spectral density curves. The spectral density curves exhibit a more rapid decrease in energy level with increasing frequency than do spectral density curves obtained from hot wire measurements. Finally, a brief literature survey has been made of the infrared properties of CO_2 and H_2O in the $2.7\,\mu$ region for small optical path lengths and elevated temperatures. The absorption data presented are especially applicable to laboratory experiments.

TABLE OF CONTENTS

NOMENCLATURE

A	area
$A_{\Delta \upsilon}$	integrated intensity of a band $\int k(\upsilon)\, d\upsilon$
B	"self" broadening coefficient
C_1	constant, 3.74×10^{-12} watt-cm^2
C_2	constant, 2.59×10^4 micron $^\circ$R
d_o	diameter of orifice
D*	cell detectivity
$E_1(n)$	one-dimensional velocity energy spectrum
Δf	bandwidth
$G_1(n)$	one-dimensional temperature energy spectrum
$k(\upsilon)$	empirical mass absorbtion coefficient
L_x	longitudinal scale of velocity fluctuation
L_y	lateral scale of velocity fluctuations
m_o	mass flow of jet
m_1	mass flow of entrained gas
n	frequency, cps
N	broadband noise
NEH	noise equivalent irradiance of the radiometer
P	jet exit pressure
P_A	absorber partial pressure
P_e	equivalent total pressure
P_F	foreign gas partial pressure
P_p	partial pressure of CO_2
q	dynamic pressure $(1/2\, \bar{\rho}\, \bar{U}^2)$
q_{max}	maximum dynamic pressure at section
r	radial distance from jet axis

$r_{1/2}$	at any section the value of r for which $\bar{U} = 1/2\ \bar{U}\ max$
$r'_{1/2}$	at any section the value of r for which $\bar{\theta} = 1/2\ \bar{\theta}\ max$
S	broadband signal
T_o	absolute initial jet temperature
T_r	absolute temperature of receiving medium
$\bar{T}$	mean absolute temperature
$\bar{T}_{max}$	maximum $\bar{T}$ at a section on jet axis
T'	r.m.s. value of temperature fluctuation
$\bar{U}_o$	initial jet velocity
$\bar{U}$	axial component of mean velocity
$\bar{U}_{max}$	maximum $\bar{U}$ at a section on jet axis
U'	r.m.s. value of axial component of velocity
w	optical path length
x	axial distance from orifice
$\alpha(\upsilon)$	spectral absorptivity coefficient
$\bar{\alpha}_{\Delta\lambda}$	mean value absorption coefficient over a band, $\Delta\lambda$
$\bar{\alpha}_{\Delta\upsilon}$	mean value absorption coefficient over a band, $\Delta\upsilon$
Δ	momentum diameter
Δ_1	constant density momentum diameter
$\Delta H'$	r.m.s. irradiance
$\Delta W'$	r.m.s. radiant emittance
Δy	thickness of radiating layer
$\overline{\Delta U}^2$	total energy of velocity turbulence
$\overline{\Delta\theta}^2$	total energy of temperature turbulence
$\epsilon(\upsilon)$	spectral coefficient of emissivity
$\bar{\theta}$	$\bar{T} - T_r$
$\bar{\theta}_o$	$T_o - T_r$
$\bar{\theta}_{max}$	maximum $\bar{\theta}$ at a section on jet axis
θ'	r.m.s. value of $\bar{\theta}$ fluctuations
λ	wavelength (microns)

MC 61-5-R5

Λ_x	longitudinal scale of temperature fluctuations
Λ_y	lateral scale of temperature fluctuations
υ	wavenumber (cm^{-1})
ρ_o	absolute initial jet density
ρ_r	absolute density of receiving medium
τ	coefficient of transmissivity
$\bar{\tau}_{\Delta\lambda}$	mean value transmissivity of a gas over a band, $\Delta\lambda$
$\bar{\tau}_{\Delta\upsilon}$	mean value transmissivity of a gas over a band, $\Delta\upsilon$
Ω	field of view of radiometer

LIST OF FIGURES

1.0 INTRODUCTION AND BACKGROUND

MITHRAS, Inc. has been actively engaged in a program directed toward determining the infrared noise emanating from a hot turbulent boundary layer. This noise resulting from small, random fluctuations in temperature and density has been termed "near field" noise and can severely limit the use of infrared sensors on board a missile or re-entry vehicle.

Theory alone, or even theory coupled with currently available experimental data, is not expected to yield near field noise predictions of high accuracy. The limiting factor is the current mathematical description of the fluctuating quantities in a turbulent boundary layer. For this reason experimental programs have been undertaken to obtain the level and nature of this noise in known turbulent environments.

In the Fall of 1963 an experiment was conducted in the hypersonic wind tunnel at the David Taylor Model Basin to measure the infrared noise generated from the hypersonic turbulent boundary layer of the wind tunnel nozzle, (Reference 1). This experiment was successful in that the RMS level of fluctuations measured were generally as predicted, but due to discrete spikes in the power spectra, questionable properties of the boundary layer and of the free shear layer observed only partial success was achieved in predicting the spectrum of the fluctuating radiation. This valuable information obtained from the DTMB experiment pointed out the desirability of a well controlled experiment for measuring the infrared noise in a well known turbulent zone. It was felt that the hot free subsonic jet would lend itself to such an experiment. Furthermore, the possibility of developing such an experiment into a laboratory tool for testing infrared sensor systems in the presence of the simulated near field background was foreseen.

Thus, efforts were directed towards developing a near field background simulator which could be employed in the MITHRAS laboratory and towards determining the infrared properties of the emitting gases to be used in the simulator over very small optical path lengths. A summary of the ensuing studies, equipment design and initial calibration follow.

<div align="center">1</div>

2.0 THE NEAR FIELD INFRARED BACKGROUND SIMULATOR

The development of a near field infrared background simulator has been undertaken, utilizing a simple heated round free subsonic jet as the infrared noise generator. The free jet has been the subject of many investigations. Some of these investigations are presented in References 2 through 6, and Hinze (Reference 7) presents a summary of free jet theory and experiments.

The above investigations have yielded power spectra of velocity and temperature fluctuation in heated and unheated jets. However, no direct measurements of the fluctuating component of the infrared signal has been measured heretofore. The development of a near field infrared background simulator therefore requires an understanding of the velocity and temperature turbulence of the hot free jet as well as direct measurements of the infrared "turbulence".

2.1 Diffusion and Spectra in the Hot Free Subsonic Jet

2.1.1 Basic Zones of the Free Jet

Figure 1 presents a schematic of the free subsonic jet. The jet immediately downstream of the exit plane contains a uniform velocity core surrounded by a turbulent mixing zone. This turbulent mixing zone grows until it covers the entire jet. At some distance further downstream the turbulent jet flow becomes fully developed and the flow patterns remain similar in consecutive sections. The location of the fully developed turbulent zone in which we are interested in making observations is not too well defined. Hinze (Reference 7) infers that although radial distributions of mean velocity and mean temperature are similar beyond $x/d_o = 10$, self preservation of the distributions of turbulent intensities is not quite fully attained at $x/d_o = 20$.

MC 61-5-R5

2.1.2 Axial Distributions of Jet Properties

The mean velocity and temperature distributions along the axis of the jet are important parameters in defining the jet. According to Hinze (Reference 5) the mean velocity distribution is given by

$$\frac{\overline{U}}{\overline{U}_{max}} = 6.4 \frac{d_o}{x + .6d_o}$$

However Corrsin and Uberoi present data in Reference 2 which shows that the hotter the jet, relative to its surroundings, the greater the jet spreading and thus the more rapid the mean velocity decay. They present evidence that the proper diameter to be used in hot jet calculations is the momentum diameter defined as

$$\Delta = 2\sqrt{2} \left(\int_o^\infty q/q_{max} \, r \, dr \right)^{1/2}$$

The ratio of the hot jet momentum diameter to the cold jet (constant density) momentum diameter, Δ/Δ_1, is presented in Figure 2. Ricou and Spalding, however present evidence that the ratio $\sqrt{\rho_r/\rho_o}$ or $\sqrt{T_o/T_r}$ may be used to make temperature corrections to the data (Reference 6). This question of a scaling parameter will be further resolved with the experimental results obtained from the current experiment.

Figure 3 presents the mean velocity distribution along the axis from the experiments of Corrsin and Uberoi (Reference 3) at $\bar{\theta}_o = 27°$ F and $\bar{\theta}_o = 540°$ F. The distribution as defined by Hinze is also included for comparison.

Similar data for the mean temperature distribution along the jet axis is shown in Figure 4.

2.1.3 Jet Cross Sections

The common way of defining the cross section of the velocity and temperature profiles are in terms of their half-value radii.

Hinze defines the half velocity radius as

$$r_{1/2} = 0.08 (x. + .6 d_o)$$

This curve has been plotted in Figure 5. Two points obtained from the Corrsin and Uberoi data at an $x/d_o = 15$ and $\bar{\theta}_o = 27°F$ and $\bar{\theta}_o = 540°F$ are also shown.

Corrsin and Uberoi presented the variation of the half-temperature radius $r'_{1/2}$, with x/d_o for $\bar{\theta}_o = 27°F$ and $\bar{\theta}_o = 540°F$. These data are shown in Figure 6.

The actual cross section distributions of the mean velocity ratio, $\overline{U}/\overline{U}_{max}$, and the R.M.S. velocity ratio of the fluctuating component, $U'/\overline{U}_{max}$, are presented in Figure 7 as obtained by Corrsin and Uberoi at $x/d_o = 15$ and $x/d_o = 20$. Also shown is the unsteady component at two radial stations and $x/d_o = 20$ for a later test by Corrsin and Uberoi. No explanation was offered for the difference in the data, but considering the nature of these measurements the agreement is considered fair.

Similar data has been plotted in Figure 8 for the mean temperature ratio $\bar{\theta}/\bar{\theta}_{max}$ and the R.M.S. temperature fluctuations $\theta'/\bar{\theta}_{max}$.

2.1.4 Scales of Turbulence

In order to define the physical eddy size of turbulent structure a correlation length or integral scale of turbulence is used. The interpretation of this scale as the mean eddy size is somewhat crude, however, it is a useful parameter for comparative purposes.

MC 61-5-R5

In terms of the normalized power spectrum of longitudinal velocity fluctuations the longitudinal velocity scale of turbulence is defined as

$$L_x = \frac{\overline{U}}{4\,\overline{\Delta U}^2}\ E(0)$$

Similarly the longitudinal temperature scale of turbulence may be defined as

$$\Lambda_x = \frac{\overline{U}}{4\,\overline{\Delta\theta}^2}\ G(0)$$

The longitudinal velocity scale of turbulence, L_x, was determined experimentally by Laurence (Reference 4) for the cold jet, $T_o/T_r = 1.0$, up to an $x/d_o = 8$. Since this is in the mixing zone, L_x is dependent upon the radial location in the jet. and thus was determined as a function of radial position as well as axial position. Corrsin and Uberoi (Reference 3) found L_x for a cold jet at $x/d_o = 20$ to be approximately constant at least up to a radial distance of 1.6 nozzle exit diameters. The above data have been normalized with respect to the nozzle exit diameter, d_o, and are plotted in Figure 9. A straight line has been drawn through the data and extrapolated by the writer to $x/d_o = 30$ for the cold jet case, $T_o/T_r = 1.0$.

The experimental data for the longitudinal temperature scale of turbulence is apparently limited to the data of Corrsin and Uberoi in Reference 3, and this data was limited to one station at $x/d_o = 20$ and $T_o/T_r = 1.6$. It was determined that for this point that $\Lambda_x \approx 0.58 L_x$ and was assumed that this relation would hold for the regions of our interest. The results of these assumptions are presented in Figure 10.

The lateral scales of turbulence are also based upon the same set of Corrsin and Uberoi data. Based upon these data it is found that $L_y \approx 1/5\,L_x$ and $\Lambda_y \approx 1/3\,\Lambda_x$.

MC 61-5-R5

2.1.5 Velocity and Temperature Spectra

The distribution of energy as a function of frequency in turbulent structure is termed a power spectrum. A mathematical description of turbulence and the power spectrum is given in Reference 8 and thus will not be repeated here. It is pointed out however, that the non-dimensional energy parameter is generally written as

$$\frac{\overline{U}\, E_1(n)}{\overline{\Delta U}^2\, L_x}$$

and the non-dimensional frequency parameter is

$$\frac{n\, L_x}{\overline{U}}$$

for the case of the one dimensional power spectrum of the x-velocity fluctuations. Similar parameters are used for temperature spectra.

In Reference 3. Corrsin and Uberoi measured the longitudinal velocity and temperature fluctuation in a free subsonic jet with a hot wire anemometer and derived the corresponding power spectra. The velocity spectra are presented in Figure 11 and the temperature spectra in Figure 12 for the axial station of $x/d_o = 20$. Also on these figures is plotted the curve described by

$$\frac{\overline{U}\, E_1(n)}{\overline{\Delta U}^2 L_x} = \frac{4}{1 + 4\pi^2 \left(\dfrac{n\, L_x}{\overline{U}}\right)^2}$$

This semi-empirical equation fits both the velocity and the temperature spectra well.

2.2 The Free Jet Noise Experiment

2.2.1 Objectives

The objective of the free jet experiment is to measure the infrared noise generated by the turbulent jet and to correlate these data with theory based upon the existing data presented in section 2.1. The experimental setup may then be used as a near field infrared background simulator to test infrared sensor systems, after slight modifications are made based upon the experimental results.

2.2.2 Apparatus

2.2.2.1 Jet and Supply

The jet is designed so as to provide a well controlled turbulent zone which may be observed with a simple AC radiometer system. A controlled amount of CO_2 may be mixed with the flow such that a sufficient signal to noise ratio may be obtained by observing the 2.7μ CO_2 and H_2O bands.

The following jet properties have been established as fulfilling the above requirements:

$$d_o = 1 \text{ inch}$$

$$A_o = 0.785 \text{ in}^2$$

$$P = 14.7 \text{ lbs/in}^2$$

$$T_r = 540°R$$

$$T_o = 1460°R$$

$$P_p/P = 0.05$$

$$\bar{U}_o = 125 \text{ ft/sec}$$

$$m_o = 0.019 \text{ #/sec}$$

MC 61-5-R5

$$\bar{\theta}_o = T_o - T_r = 920°F$$

$$T_o/T_r = 1/\rho_o/\rho_r = 2.7$$

In order that the jet characteristics of section 2.1 may be valid, it is necessary that the jet issue into an environment of the same gas composition as the jet itself, i.e. $P_p/P = 0.05$. The environment is controlled by letting the jet issue into a chamber in which the mass flow entrained by the jet will be replaced. Ricou and Spaulding (Reference 6) have empirically shown that the mass flow entrained by a jet issuing into an environment of different density is given by the relation

$$m_1 = m_o \left[0.32 \, x/d_o \, (\rho_r/\rho_o)^{1/2} - 1\right]$$

Assuming that the total length of the jet we are interested in is 30 inches, then $x/d_o = 30$ and $m_1 = 0.28 \, \#/sec$. If the jet is issued in an upward direction the data of Ricou and Spaulding show that the effects of buoyancy on the proposed jet experiment will introduce negligible flow entrainment.

A schematic diagram of the test set-up is presented in Figure 13. Ricou and Spaulding have shown that the aperture angle subtended by the diameter of the chamber outlet aperture, should be about 30° in order to assure minimum interference with the jet and zero pressure gradient between the chamber and the atmosphere. The pressure ratio across the aperture, P_1/P_2, will be measured and balanced with valves V_1 and V_2.

Valves V_3 and V_4 control the air - CO_2 mixture, part of which is heated with a 7 kw heater.

The air supply is drawn from room air by a centrifugal blower which has a one horse-power motor and provides a pressure rise of 6" of water. The heater is a 7 kw. three stage unit utilizing GE calrods as the heating elements.

MC 61-5-R5

2.2.2.2 Radiometer

For simplicity in estimating the irradiance of the jet, it will be assumed that the jet cross section being observed is of constant mean temperature and may be treated as a body of gas of thickness Δy and of uniformly fluctuating temperature. The absorptivity, $\alpha(\upsilon)$, of this gas may be controlled by the CO_2 partial pressure and will be limited to $\alpha(\upsilon) = 0.25$. This is the criterion assumed for optically thin layers for which the Beer-Lambert law,

$$\alpha(\upsilon) = 1 - e^{-k(\upsilon)w}$$

may be approximated as

$$\alpha(\upsilon) = k(\upsilon) w$$

the total absorption of a band, $\Delta\upsilon$, may be written as

$$\int \alpha(\upsilon) \, d\upsilon = w \int k(\nu) \, d\nu = w A_{\Delta\nu}$$

and the mean value absorption over a given bandwidth is

$$\bar{\alpha}_{\Delta\upsilon} = \bar{\alpha}_{\Delta\lambda} = \frac{1}{\Delta\upsilon} \int \alpha(\upsilon) \, d\upsilon = \frac{w}{\Delta\nu} \int k(\nu) \, d\nu = \frac{w}{\Delta\nu} A_{\Delta\nu}$$

Values of the total absorption of CO_2 and H_2O over the 2.7μ band are compiled in section 3.0.

Due to the spectral shape of the absorption curve in the 2.7μ region, the mean value absorption must be limited to approximately $\bar{\alpha}_{\Delta\upsilon} = 0.15$ from a wavenumber of 3500 cm^{-1} to 3800 cm^{-1} (2.85μ to 2.63μ) in order for the maximum $\alpha(\upsilon)$ to be limited to 0.25.

According to Kirchoff's law the spectral absorptivity and emissivity of the gases are equal,

$$\alpha(\upsilon) = \epsilon(\upsilon)$$

MC 61-5-R5

An estimate of CO_2 concentration in dry air to make $\bar{\alpha}_{\Delta \upsilon} = 0.15$ may be made from the total absorption data of Figure 21 which is discussed in section 3.0. It is estimated that about a 5% CO_2 concentration would yield $\bar{\alpha}_{\Delta \upsilon} = \bar{\alpha}_{\Delta \lambda} = 0.15$ and the peak $\alpha(\upsilon) = 0.25$. An accurate estimate is complicated however by the fact that the temperature varies across the jet and the Δy taken as 8 inches is somewhat ficticious. For these reasons, the CO_2 concentration may be varied during the experiment.

The jet is observed through a layer of surrounding gas of the same CO_2 concentration and also of thickness Δy (8 inches). Therefore the mean value transmissivity of the gas is taken as

$$\bar{\tau}_{\Delta \lambda} = 1 - \bar{\alpha}_{\Delta \lambda} = /0.85$$

The equations for the R.M.S. intensity, $\Delta W'$, of the fluctuation in radiant emittance over a narrow bandwidth is given in Reference 1. Rewriting these equations in the appropriate form yields

$$\Delta W' = \frac{T'}{\bar{T}} \quad \frac{C_1}{\bar{\lambda}^5} \left[\frac{1+(C_2/\bar{\lambda}\bar{T} -1)e^{C_2/\bar{\lambda}\bar{T}}}{(e^{C_2/\bar{\lambda}\bar{T}} -1)^2} \right] \bar{\alpha}_{\Delta \lambda} \Delta \lambda$$

The irradiance falling on the radiometer detector is

$$\Delta H' = \Delta W' \frac{\Omega}{2\pi} \bar{\tau}_{\Delta \lambda}$$

this total irradiance will be solved for at an $x/d_o = 20$, a likely region to look at in this experiment. At $x/d_o = 20$ and for the jet properties listed in section 2.2.2.1 we find from section 2.1,

$$\frac{\bar{\theta}_{max}}{\bar{\theta}_o} = .15$$

$$\frac{\theta'}{\bar{\theta}_{max}} = .14$$

$$\bar{T} = 678°R$$

$$\theta' = T' = 19°F$$

$$\frac{T'}{\bar{T}} = .028$$

On the jet centerline

and

$$\frac{\theta'}{\bar{\theta}_{max}} = .16$$

$$\bar{T} = 609°R$$

$$\theta' = T' = 22°F$$

$$\frac{T'}{\bar{T}} = .036$$

At $r/r'_{1/2} = 1.0$
or 2.75 inches from
the jet centerline

and

$$\frac{\theta'}{\bar{\theta}_{max}} = .10$$

$$\bar{T} = 576°R$$

$$\theta' = T' = 14°F$$

$$\frac{T'}{\bar{T}} = .024$$

At $r/r'_{1/2} = 1.5$
or 4.1 inches from
the jet centerline

11   MC 61-5-R5

Average properties will be used in calculating the irradiance and taken as $\bar{T} = 600°R$ and $T'/\bar{T}_{max} = 0.031$.

The radiometer will be assumed identical to the A.C. radiometer used in the experiments of Reference 1. This radiometer was found in Reference 1 to have a field of view of $\Omega = 0.076$ steradians.

Using the above values we find

$$\Delta W' = 5.66 \times 10^{-7} \text{ watts/cm}^2$$

$$\Delta H' = 5.85 \times 10^{-9} \text{ watts/cm}^2$$

In order to establish the possibility of obtaining good data from the experiment proposed, the broad-band signal-to-noise ratio will be computed. Conventionally the signal-to-noise ratio is equal to the irradiance falling on the detector divided by the noise equivalent irradiance of the radiometer,

$$S/N = \frac{\Delta H'}{NEH}$$

where

$$NEH = \frac{(A_D)^{1/2}(\Delta f)^{1/2}}{A_{collector} D^*}$$

The detector used will be the Infrared Industries type B1 detector described in References 10 and 11. This detector has a time constant less than 60μ sec and the peak D^* at 3000 cps is 10^{11} cm(cps)$^{1/2}$/watt at room temperature. In the narrow bandwidth from which the radiation comes from we may assume monochromatic radiation at 2.73μ. At this wavelength $D^*/D^*_{peak} = 0.45$.

The radiometer system used here has a detector area A_D = 0.4 cm^2 and a collector area $A_{coll.}$ = 18 cm^2. The bandwidth will be taken as 40,000 cps such that $(\Delta f)^{1/2}$ = 2 x 10^2 (cps)$^{1/2}$ the noise equivalent irradiance is computed to be

$$NEH = 1.56 \times 10^{-10} \text{ watt/cm}^2$$

$$\therefore S/N = 37.5$$

This is considered a good broad band signal to noise ratio for such an experiment.

2.2.3 Instrumentation

The instrumentation consists of pressure and temperature instrumentation shown in the schematic of Figure 13 and electronics and data readout equipment to record the data.

The pressure and temperature instrumentation is designed such that a proper ratio of CO_2 may be maintained and the jet flow conditions such as velocity, pressure, and temperature may be well controlled. The instrumentation for this phase is considered quite routine.

The total radiation signal will be received from the pre-amplifier on the A.C. radiometer and analyzed on a Hewlett-Packard wave analyzer.

2.3 Initial Calibration of the Near Field Infrared Background Simulator

A preliminary initial calibration of the jet noise experiment described in section 2.2 has been made. The purpose of this calibration was to confirm the aerodynamic predictions based upon the data of section 2.1 and to establish that an adequate signal for analysis could be obtained from the A.C. radiometer.

The results from this initial calibration follow.

2.3.1 Aerodynamic Measurements

The hot jet was calibrated using an external pitot probe
and thermocouple probe as shown schematically in Figure 14. As a
result of this calibration it is estimated that during operation the jet
velocity will be known within ± 2 ft/sec and the stagnation temperature
will be accurate within $\pm 10°F$.

The results of a survey of the axial decay of the centerline velocity,
$\overline{U}_{max}$, is presented in Figure 15 for the cold jet, $\bar{\theta}_o = 0°F$, and for two
elevated temperatures $\bar{\theta}_o = 535°F$ and $\bar{\theta}_o = 960°F$. $\bar{\theta}_o$ is the temperature
difference between the initial jet stagnation temperature and the surround-
ing environment, $T_o - T_r$. Note the excellent agreement with the data of
Corrsin and Uberoi (Reference 2). This data may be collapsed into a
single curve by using $\chi/d_o \sqrt{T_o/T_r}$ as the ordinate as shown in Figure 16.

The results of the axial decay of the centerline temperature differ-
ence, θ_{max}, is presented in Figure 17 for $\bar{\theta}_o = 535°F$ and $\bar{\theta}_o = 960°F$.
This data also shows good agreement with the data of Corrsin and Uberoi.

2.3.2 Radiometric Measurements

Radiometric measurements were made for the hot jet,
$\bar{\theta}_o = 950°F$, at distances from the nozzle exit of $\chi/do = 5.5, 10, 15$,
and 20. The A.C. radiometer with a PbS cell was located approximately
6 1/2 inches from the jet centerline. A brief field of view survey showed
about a one inch field of view on the jet centerline. No foreign gas was
used in the jet so that the radiometric response was due primarily to the
2.7μ H_2O band. At the time of the runs the H_2O content of the air was
approximately 1.9 percent.

The total radiation signal received from the pre-amplifier on the
A.C. Radiometer was analyzed on a Hewlett-Packard wave analyzer with
a fixed bandwidth of $\delta_n = 7$ cps. This signal plus noise voltage, $v_{S+N}(n)$,
when squared and divided by the bandwidth represents approximately the
energy in the fluctuations of the radiation signal at a given frequency. The
data included herein was not corrected for the noise signal which was low

nor for the frequency response of the radiometer since it is flat to 3 db below 3000 cps. The energy spectra of the radiation signals is plotted in Figure 18.

The total energy in the fluctuations of the radiation signal can be computed from the total RMS voltage, V, of the pre-amplifier output given by

$$V^2 = \frac{1}{\delta_n} \int v^2_{S+N}(n) \, dn$$

Note that V^2 is given by the total area under the curves in Figure 18. The total RMS voltage is presented in Figure 19 as a function of distance from the nozzle exit plane. Once this total has been obtained, it may be used to normalize the power spectrum of the fluctuations and to obtain the spectral energy density.

$$E(n) = \frac{v^2_{S+N}(n)}{\delta_n V^2}$$

The data of Figure 18 has been replotted in Figure 20 in a normalized form as a function of a pseudo-wavenumber, $n\overline{U}_{max}$.

The radiation energy spectra exhibit different characteristics than the energy spectra of the temperature fluctuations of Corrsin and Uberoi (Reference 3). The radiation energy falls off much more rapidly at higher frequencies than the energy of the temperature fluctuations. This phenomenon is believed to be due to the aperture-signal interaction and will be investigated in the future in greater detail.

The longitudinal scale of turbulence is normally defined as

$$L_x = \frac{\overline{U} \, E(o)}{4}$$

and has always been considered a linear function of axial distance in the case of a free subsonic jet. The data presented shows that although the axial distance varies from $\chi/do = 5.5$ to $\chi/do = 20.0$, a factor of 3.6,

15   MC 61-5-R5

the scale of turbulence is nearly constant. If the value of $\bar{U}_{max}E(n)$ at $n/\bar{U}_{max} = 1.75$ is used to define L_x we find that $L_x \approx 1.0$ inches, the approximate field of the radiometer. The scale of turbulence will be further investigated in the future, in particular to ascertain if the field of view significantly affects these results.

2.3.3 Conclusions from Initial Calibration

The initial calibration of the near field simulator has demonstrated the feasibility of obtaining a well controlled turbulent environment in the laboratory to produce a near field A.C. signal.

The aerodynamic characteristics of the jet were essentially as predicted from the data of Corrsin and Uberoi.

The radiometric measurements indicate two significant findings:

1)   The radiation energy spectra exhibit significantly less high frequency energy than the temperature energy spectra.

2)   The longitudinal radiation scale of turbulence is nearly constant in the region of $\chi/do = 5.5$ to $\chi/do = 20.0$.

These initial findings with respect to the characteristics of the infrared signal point to the necessity for a rather thorough continued investigation of the free jet radiation. The results also point up the inadequacy which may be expected of theories developed at this time to predict the near field infrared noise.

3.0 INFRARED PROPERTIES OF CO_2 AND H_2O IN THE 2.7 μ REGION FOR SMALL OPTICAL PATH LENGTHS AND ELEVATED TEMPERATURES

Laboratory experiments in infrared technology frequently require a knowledge of the infrared absorption of CO_2 and H_2O for small optical path lengths where limited experimental data exists. The noise simulator and the turbulent boundary layer encountered in flight both emit over very small optical path lengths. For this reason a brief survey has been made of available data on total absorption for CO_2 and H_2O in the 2.7 μ region for small optical path lengths, a large range of total pressures and a large range of temperatures.

References 9 and 12 through 17 provide data on CO_2 absorption and References 9, 15, and 17 through 19 are sources of H_2O absorption data.

3.1 General

The simplest formula for describing the absorption of a gas is the Beer-Lambert law,

$$\alpha (\upsilon) = 1 - e^{-k(\upsilon)w}$$

where $\alpha(\upsilon)$ is the spectral absorptivity, $k(\upsilon)$ is the mass absorption co-efficient and w is the optical path length generally expressed in standard atmosphere-centimeters

$$w = P_A$$

For a gas at small optical path lengths $\alpha (\upsilon) \ll 1$, and we may write

$$\alpha (\upsilon) \approx k(\upsilon) w$$

The total absorption of a band, $\Delta \upsilon$, may now be written as

$$\int \alpha (\upsilon) \, d\upsilon = w \int k(\upsilon) \, d\upsilon = w A_{\Delta \upsilon}$$

where $A_{\Delta \upsilon}$ or $\int k(\upsilon) \, d\upsilon$ is generally termed the integrated band intensity.

The mean value absorption over a given bandwidth is a useful parameter in laboratory work and may be written

$$\bar{\alpha}_{\Delta \upsilon} = \frac{1}{\Delta \upsilon} \, ' \int \alpha(\upsilon) \, d\upsilon$$

for any optical path length. For small optical path lengths $\bar{\alpha}_{\Delta \upsilon}$ may be expressed in terms of the integrated intensity,

$$\bar{\alpha}_{\Delta \upsilon} = \frac{1}{\Delta \upsilon} \, w \int k(\upsilon) \, d\upsilon$$

3.2 CO_2 Absorption in the 2.7μ Region

Howard, et. al. in Reference 12 present total absorption data in the band $\Delta \upsilon = 3500 \text{ cm}^{-1}$ to 3800 cm^{-1} ($\Delta \lambda = 2.63\mu$ to 2.85μ) for equivalent total pressures of 25 mm. to 1600 mm and optical path lengths of $w = 0.08$ atm. cm. to 24 atm. cm. These data have been plotted in Figure 21 on log-log paper and extrapolated to $w = 0.001$ atm. cm.

The equivalent total pressure, Pe, is defined as

$$Pe = P_F + B P_A$$

where

P_F = foreign gas partial pressure

P_A = absorber partial pressure

B = the "self-broadening coefficient"

The equivalent total pressure is used as a single variable to account for the fact that a binary mixture is known to depend on the partial pressure, P_A, of the absorber as well as upon the total pressure of the mixture. For the 2.7μ CO_2 band. Howard et. al. has determined B to be 1.30.

Note that the total absorption curves for different values of P_e are shown in Figure 21 to converge to a maximum slope of unity with decreasing w. The asymptotic slope is shown as a dotted line and yields the total intensity of $\int k(\upsilon)\, d\upsilon = 90\ \text{atm}^{-1}\text{cm}^{-2}$. It should be noted that the temperature of the samples for these data were all near room temperature.

Limited data for high temperatures were recorded by Tourin and Henry (Reference 9) along with low temperature data. These data, corrected to standard temperature are plotted on Figure 21. Note that the data for T = 540°R falls in agreement with the data of Howard, et. al. Of major significance however, is the fact that the data for T = 2300°R and P_e = 65 mm and P_e = 715 mm at w = 0.2 atm cm falls close to the asymptotic slope of $\int k(\upsilon)\, d\upsilon$. The other high temperature data point at P_e = 910 mm and w = 3.0 atm cm also falls closer to the asymptote than the low temperature data. It appears that, at least in this temperature range the effect of increasing temperature is to delay the total absorption "breakaway" from the asymptote which occures with increasing optical path length. One would also conclude that the integrated intensity, $\int k(\upsilon)\, d\upsilon$, is roughly constant in this temperature range.

Malkmus (Reference 13) and Breeze and Ferriso (Reference 14) have compiled data for the integrated intensity in the temperature range of 500°R to 5500°R. This compilation of data from Malkmus is shown in Figure 23 and indicates that the integrated intensity is roughly constant with increasing temperature up to about 1000°R but increases thereafter.

3.3 H_2O Absorption in the 2.7μ Region

The total absorption data in the 2.7 μ region for H_2O of Burch, et. al. (Reference 15) have been plotted in Figure 22 in a manner similar to the CO_2 plot. These data, covering a range of P_e from 20 mm to 760 mm and a range of optical path length $\underline{w}$ of 0.003 pr. cm to 1.0 pr. cm. (4.85 atm cm to 1613 atm cm) have been extrapolated to an optical path length of 0.0001 pr. cm. The equivalent total pressure P_e was previously defined. However, Burch et. al. have determined B to be 5.0 for the 2.7μ band of H_2O.

Figure 22 also shows data from Ferriso and Ludwig (Reference 18) and data from Goldstein (Reference 19). These data, although at high temperatures, appear to be consistent with the data of Burch, et. al. It was not possible to determine the asymptotic value of $\int k(\upsilon)\, d\upsilon$ from the data of Burch, et. al., however the data of Goldstein at very large equivalent total pressures do provide an asymptote consistent with the other data.

A summary of integrated intensity data in the 2.7μ band of H_2O in the temperature range of 500°R to 4500°R is shown in Figure 23. Note the wide scatter in the data compared to the CO_2 data. Considering this scatter, it is difficult to conclude whether the $\int k(\upsilon)\, d\upsilon$ really varies in this temperature range, but it appears that it does not.

4.0 CONCLUSIONS

Studies on the near field infrared background noise problem have been directed towards the simulation of the infrared noise emanating from a known turbulent zone.

A laboratory tool for simulating the near field noise has been designed and demonstrated successfully. This simulator was designed around the subsonic jet which is subsequently being studied for the purpose of analyzing the infrared signal emanating from this known source of turbulence. Two significant results followed from the initial studies of the subsonic jet:

1) The radiation energy spectra exhibit different characteristics than do the energy spectra of the temperature or velocity fluctuations. The radiation energy falls off much more rapidly at higher frequencies than the energy of the temperature or velocity fluctuations obtained previously in hot wire experiments.

2) The longitudinal scale of turbulence was nearly constant out to a distance of twenty nozzle exit diameters from the jet exit plane. This result is contrary to the generally accepted theory that the longitudinal scale of turbulence varies directly with distance from the nozzle.

It is concluded from these initial studies on the subsonic jet that the jet may be developed into a near field noise simulator to test infrared detector systems. However, more extensive experimental investigations into the infrared characteristics of the jet are required in order that a theory may be developed to predict the equivalent noise emanating from other zones of turbulence such as the hot turbulent boundary layer.

MC 61-5-R5

A brief literature survey of infrared properties of CO_2 and H_2O in the 2.7 μ region for small optical path lengths and elevated temperatures was conducted. The data on total absorption has been plotted versus optical path length in a region such that it may be readily applied toward laborato_y experiments or in flight boundary layers. As a result of this survey it is concluded that limited but adequate data does exist for the total absorption of CO_2 and H_2O in the 2.7 μ region for the unusually small optical path lengths encountered in laboratory or in flight near field infrared noise problems.

REFERENCES

1. Lorah, Lawrence D., Hill, Jacques A. F., and Draper, James S.: " A Wind Tunnel Measurement of Fluctuations in Infrared Emission from a Turbulent Mixing Layer (U)" MITHRAS Report MC 61-14-R2, September, 1964. (Confidential).

2. Corrsin, Stanley and Uberoi, Mahinder S.: "Further Experiments on the Flow and Heat Transfer in a Heated Turbulent Air Jet" NACA Rept. 998, 1950.

3. Corrsin, Stanley and Uberoi, Mahinder S.: "Spectra and Diffusion in a Round Turbulent Jet", NACA Rept. 1040, 1951.

4. Laurence, James C.: " Intensity, Scale, and Spectra of Turbulence in Mixing Region of Free Subsonic Jet", NACA Rept. 1292, 1956.

5. Hinze, J. O. and Van Der Hegge Zijnen, B. G.:"Transfer of Heat and Matter in the Turbulent Mixing Zone of an Axially Symmetrical Jet", Applied Science Research, 1A, 435, 1949.

6. Ricou, F. P. and Spalding, D. B.:"Measurements of Entrainment by Axisymmetrical Turbulent Jets", Journal of Fluid Mechanics 11, 21, August 1961.

7. Hinze, J. O.: "Turbulence", McGraw Hill, New York 1959.

8. Hill, J. A. F.:"Density and Temperature Fluctuations in Turbulent Boundary Layers", MITHRAS Memo 261, February 1963.

9. Tourin, R. and Henry, P.:" Infrared Spectral Emissivities and Internal Energy Distributions of Carbon Dioxide and Water Vapor at High Temperatures", Geophysics Research Directorate Report AFCRC TR-60-203, December, 1959.

10. Wieting, Terrence J.:" Visible and Infrared Detectors: State of the Art", MITHRAS Memo 172, April 1962.

11. Infrared Industries. "Photoconductors", Technical Bulletin No. 7.

12. Howard, Burch, and Williams: " Near Infrared Transmission through Synthetic Atmospheres", AFCRC-TR-55-213, November 1955.

13. Malkmus,: "Infrared Emissivity of Carbon Dioxide $(2.7\mu$ Band)", Journal Optical Soc. of Am. Vol. 54 No. 6, page 751, June 1964.

REFERENCES

14. Breeze and Ferriso,:" Shock-Wave Integrated Intensity Measurements of the 2.7 1 Micron CO_2 Band Between 1200°K and 3000°K", Journal of Chemical Physics, Vol. 39, No. 10 Page 2619, 15 Nov. 1963.

15. Burch, Gryvnak, Singleton, France, and Williams,: "Infrared Absorption by Carbon Dioxide, Water Vapor, and Minor Atmospheric Constituents", AFCRL-62-698, July 1962.

16. Burch, Gryvnak, and Williams,: " Infrared Absorption by Carbon Dioxide", Scientific Report II, Contract AF 19(604)-2633, Geophysics Research Directorate, Air Research and Development Command 1960.

17. Zachor,: "Near Infrared Transmission Over Atmospheric Slant Paths, MITHRAS, Reprinted from MIT Inst. Lab. Report-R-328, Vol. 2 July 1961.

18. Ferriso and Ludwid, :"Spectral Emissivities and Integrated Intensities of the 2.7μ H_2O Band Between 530°K and 2200°K Journal Quant. Spectrosc. Radiation Transfer page 215, Jan/Feb. 1964.

19. Goldstein, : "Measurement of Infrared Absorption by Water Vapor at Temperature to 1000°K", Journal Quant. Spectrosc. Radiation Transfer, Vol. and page 343, March/April 1964.
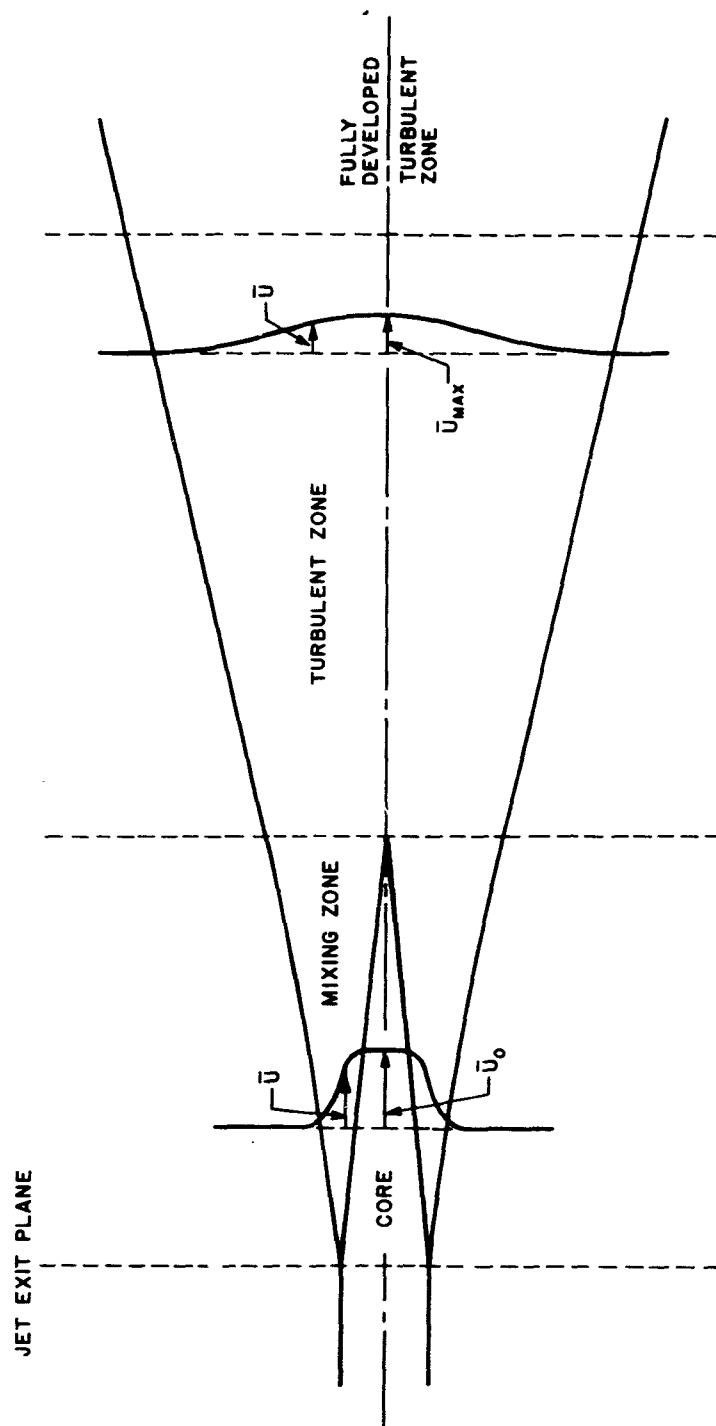
Figure 1. Schematic of the free subsonic jet

MC 61-5-R5
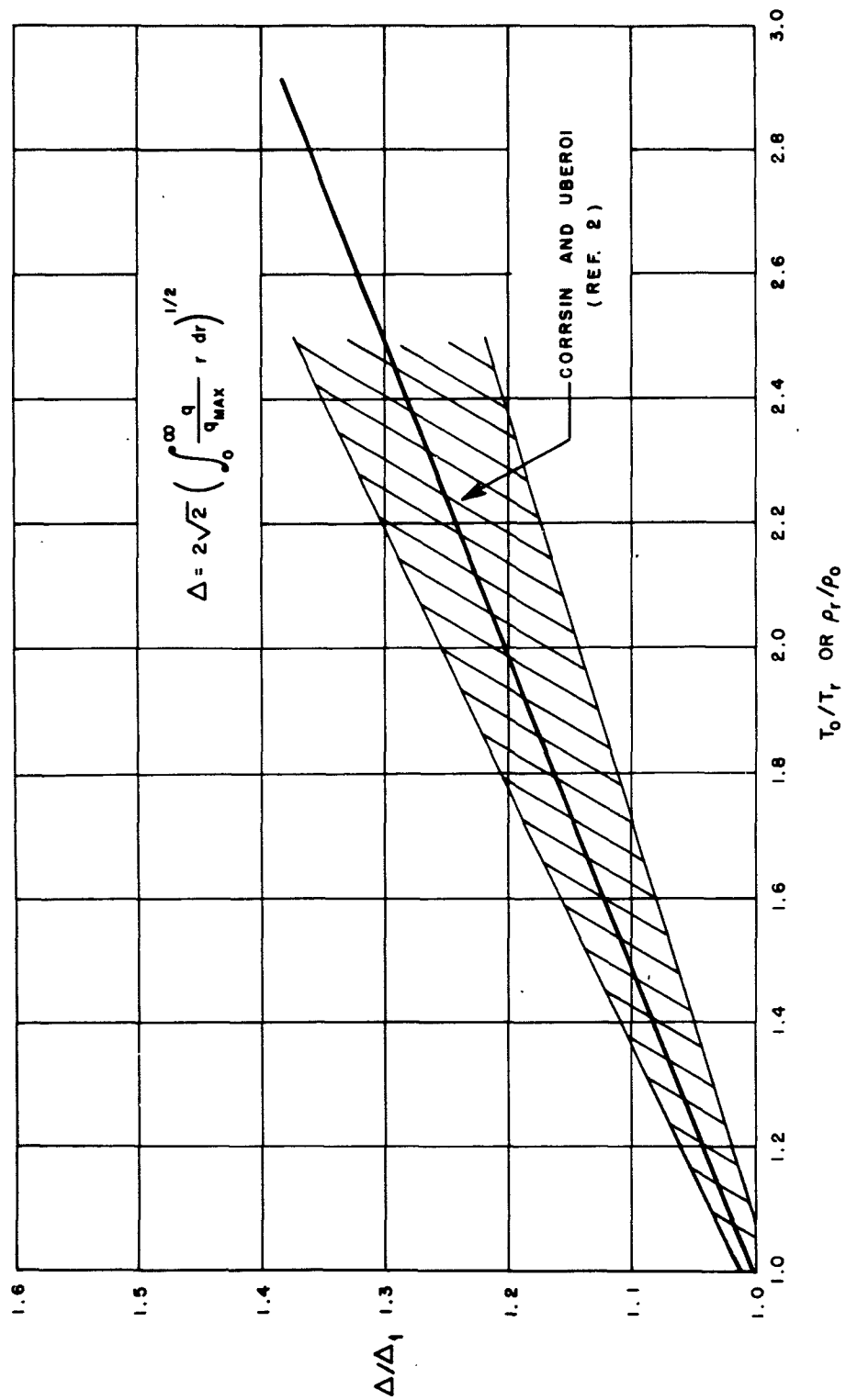
Figure 2. Variation of momentum diameter

The graph shows Δ/Δ_1 on the vertical axis (ranging from 1.0 to 1.6) versus T_0/T_r OR ρ_r/ρ_0 on the horizontal axis (ranging from 1.0 to 3.0).

$$\Delta = 2\sqrt{2}\left(\int_0^\infty \frac{q}{q_{MAX}} r \, dr\right)^{1/2}$$

CORRSIN AND UBEROI (REF. 2)

MC 61-5-R5
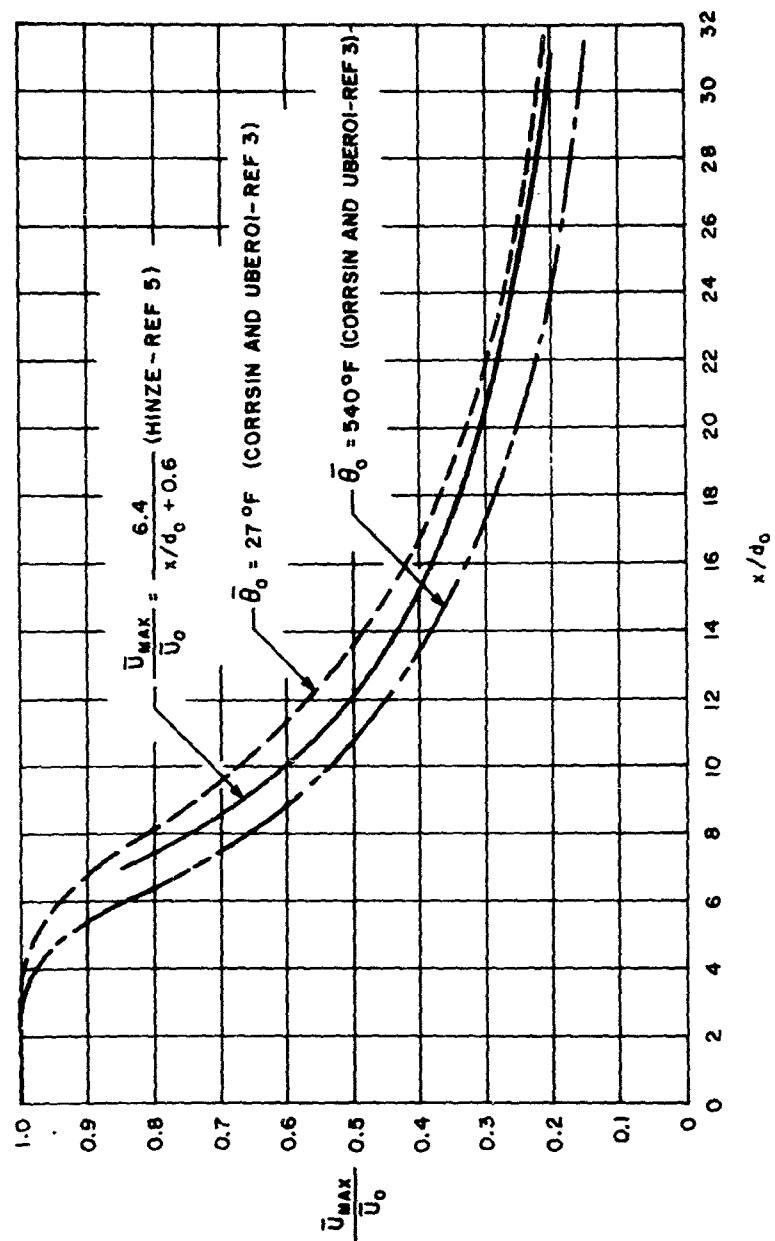
Figure 3. Axial velocity distributions
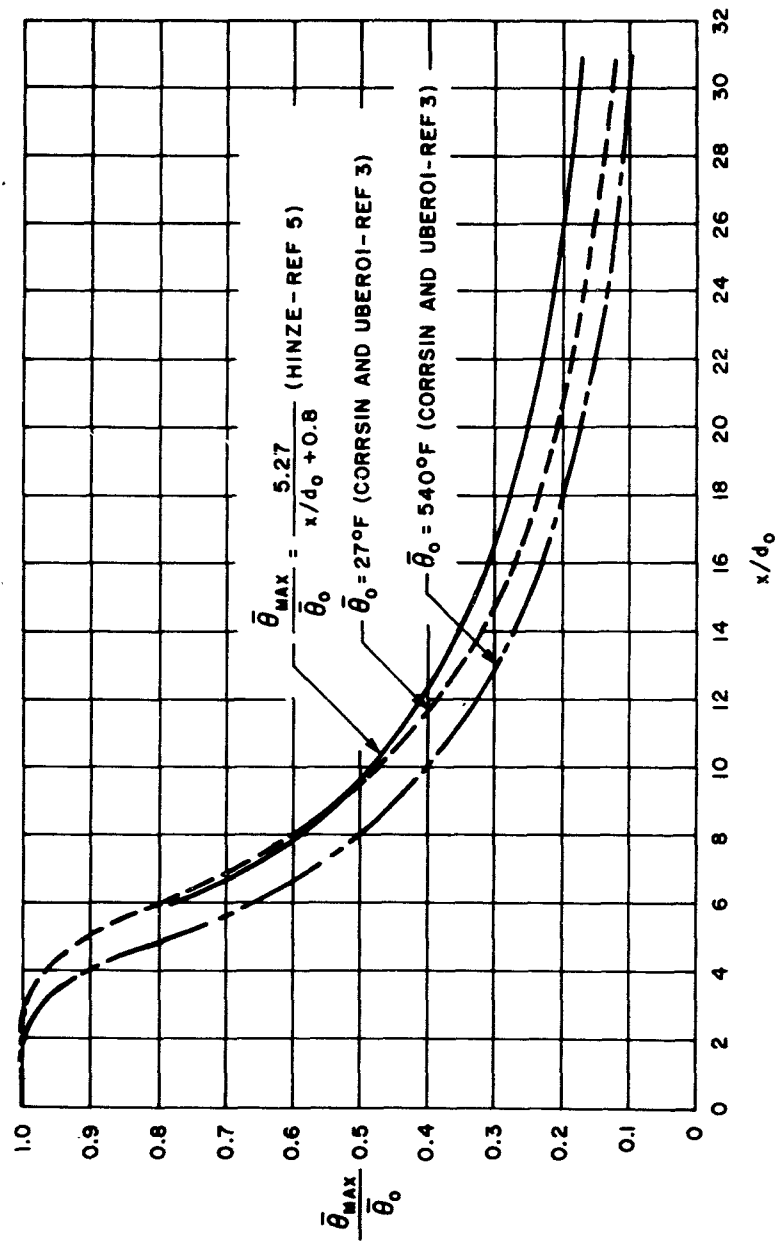
27   MC 61-5-R5

Figure 4. Axial temperature distributions

The chart shows $\frac{\bar{\theta}_{MAX}}{\bar{\theta}_o}$ (vertical axis, from 0 to 1.0) plotted against x/d_o (horizontal axis, from 0 to 32).

$$\frac{\bar{\theta}_{MAX}}{\bar{\theta}_o} = \frac{5.27}{x/d_o + 0.8} \quad (\text{HINZE} - \text{REF 5})$$

$\bar{\theta}_o = 27°F$ (CORRSIN AND UBEROI - REF 3)

$\bar{\theta}_o = 540°F$ (CORRSIN AND UBEROI - REF 3)

28
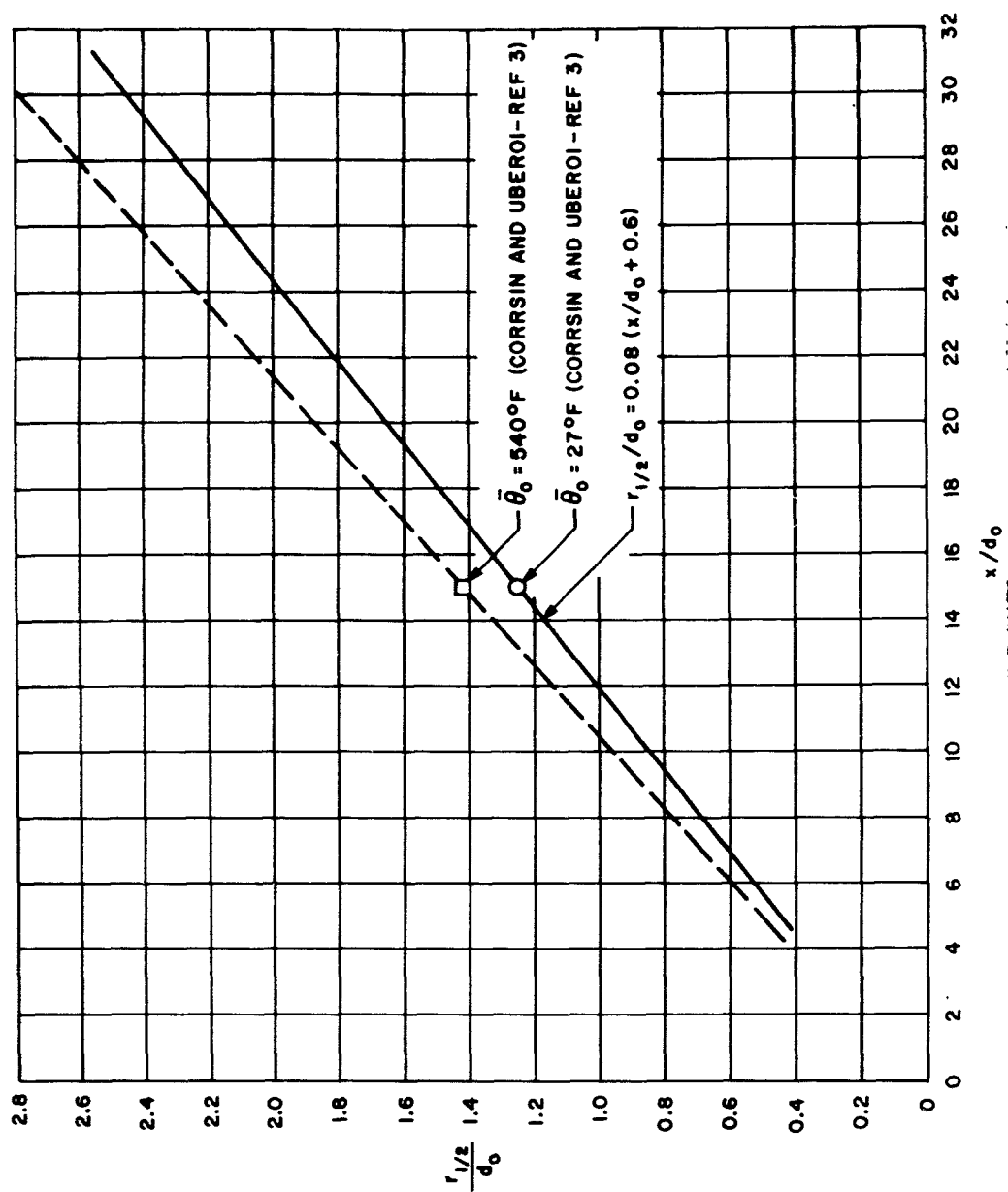
Figure 5. Axial spread of velocity
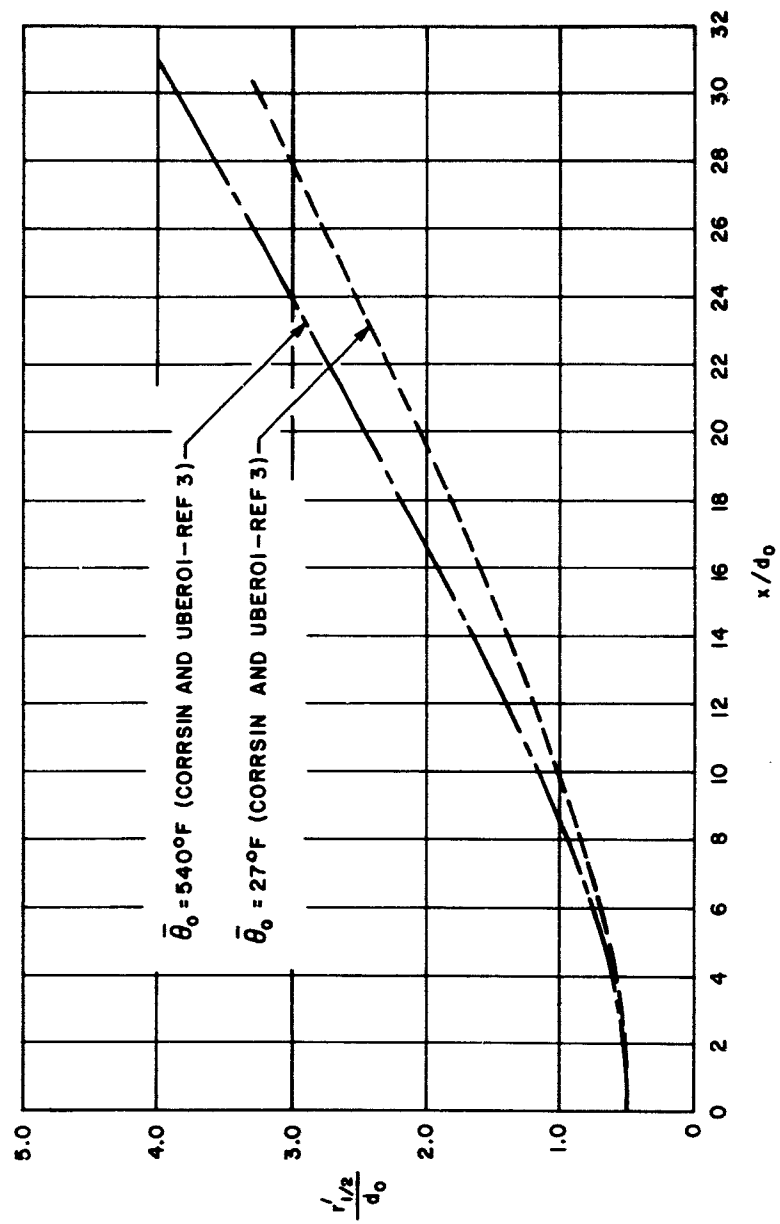
MC 61-5-R5

Figure 6. Axial spread of temperature
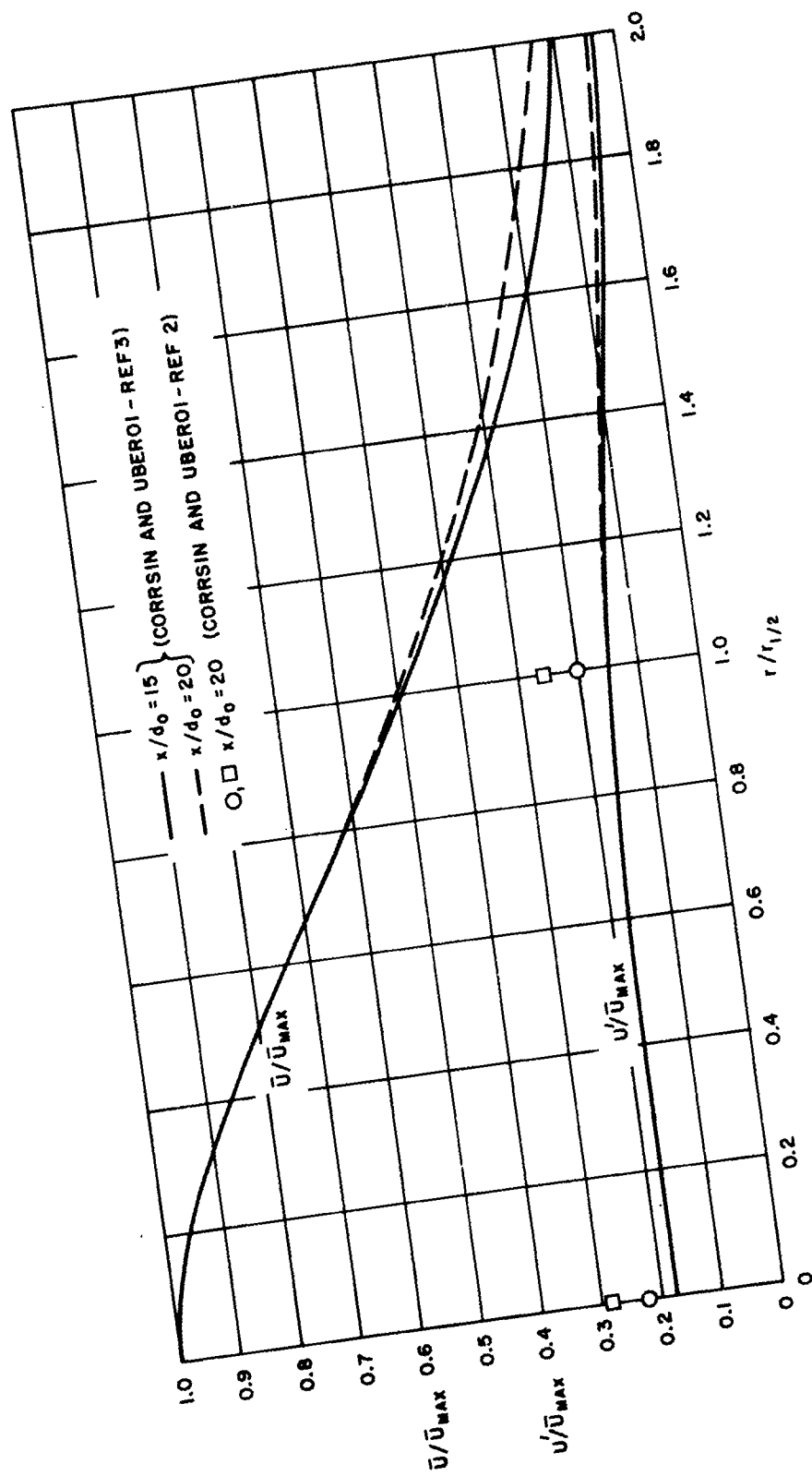
MC 61-5-R5

Figure 7. Velocity distribution and fluctuation levels in the jet cross section

MC 61-5-R5

31
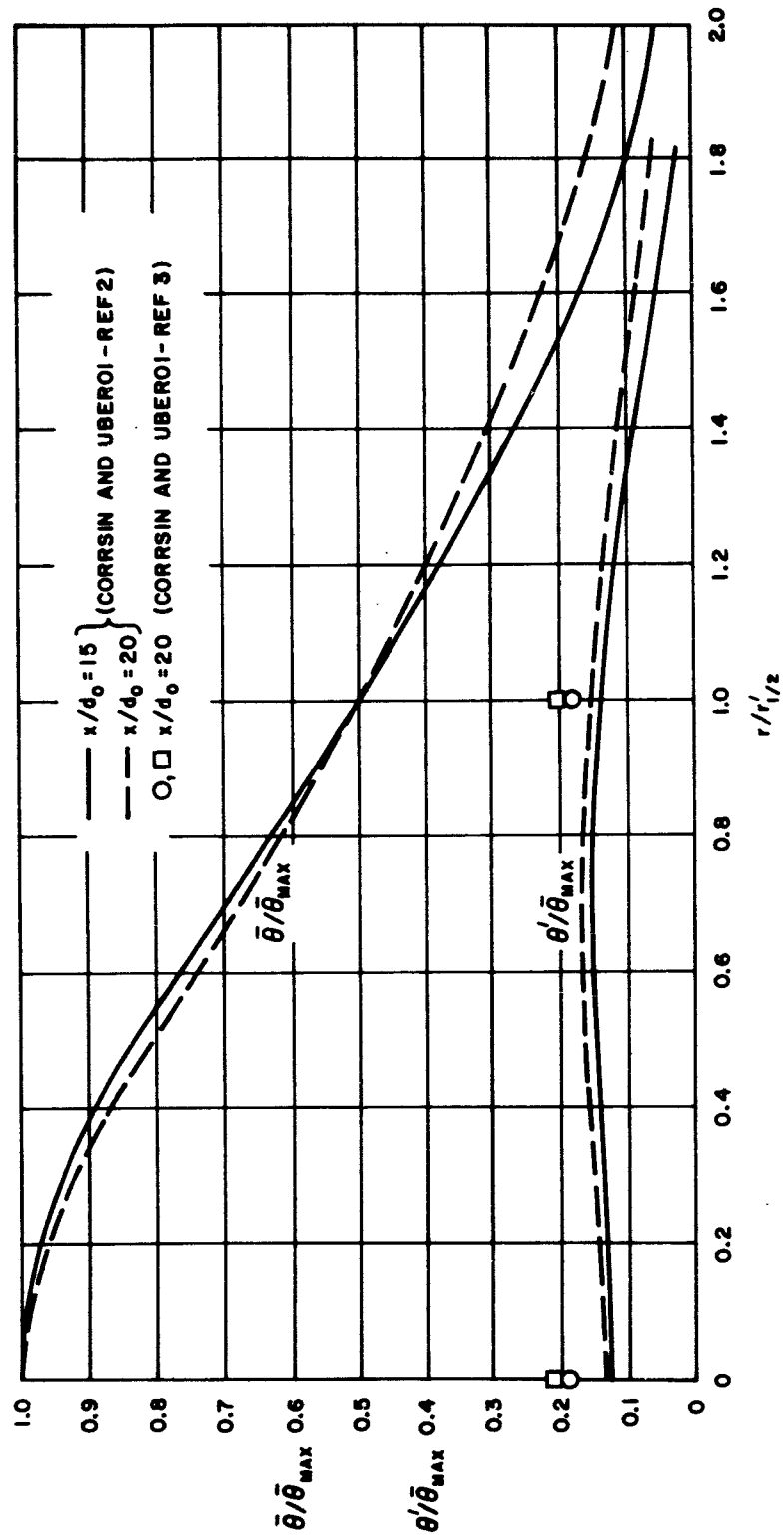
Figure 8. Temperature distribution and fluctuation levels in the jet cross section

MC 61-5-R5
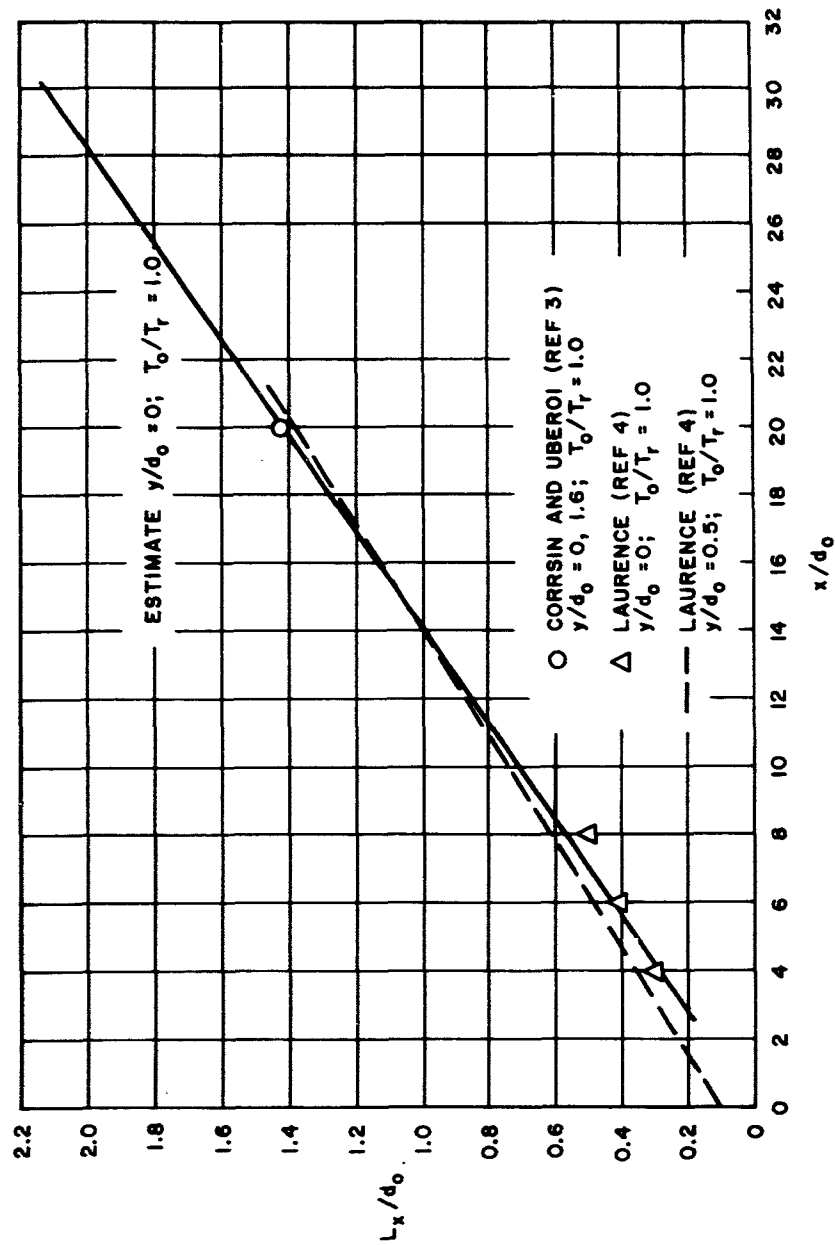
Figure 9. Longitudinal velocity scale of turbulence

33
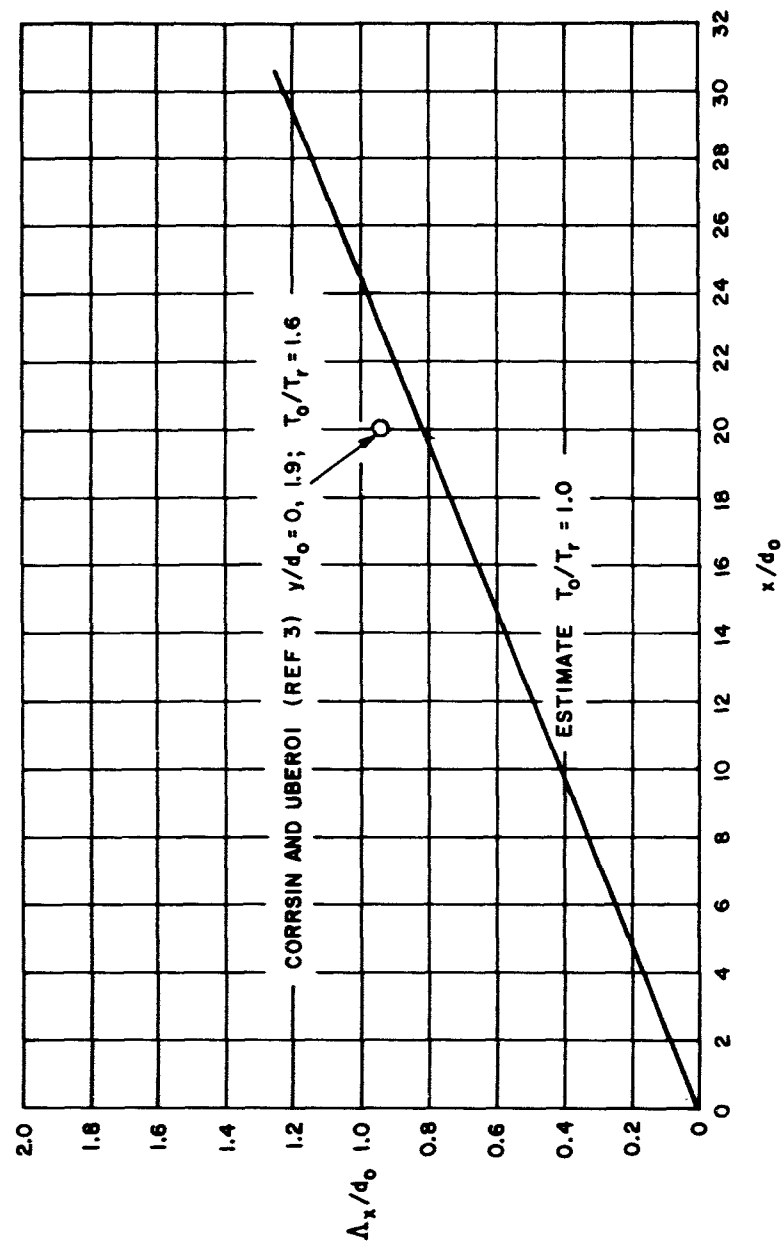
Figure 10. Longitudinal temperature scale of turbulence

MC 61-5-R5
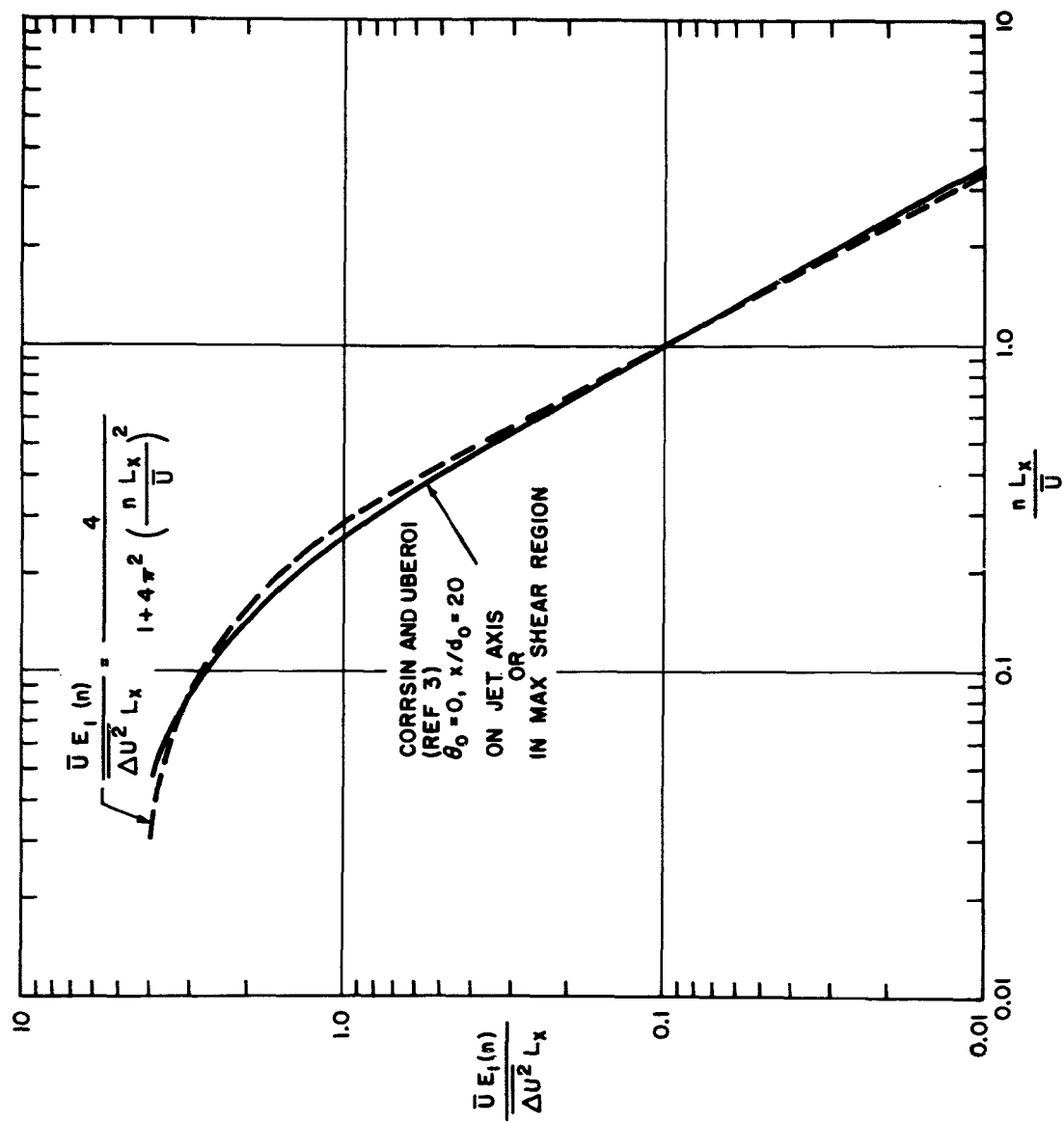
Figure 11. Power spectra of velocity fluctuations

35   MC 61-5-R5
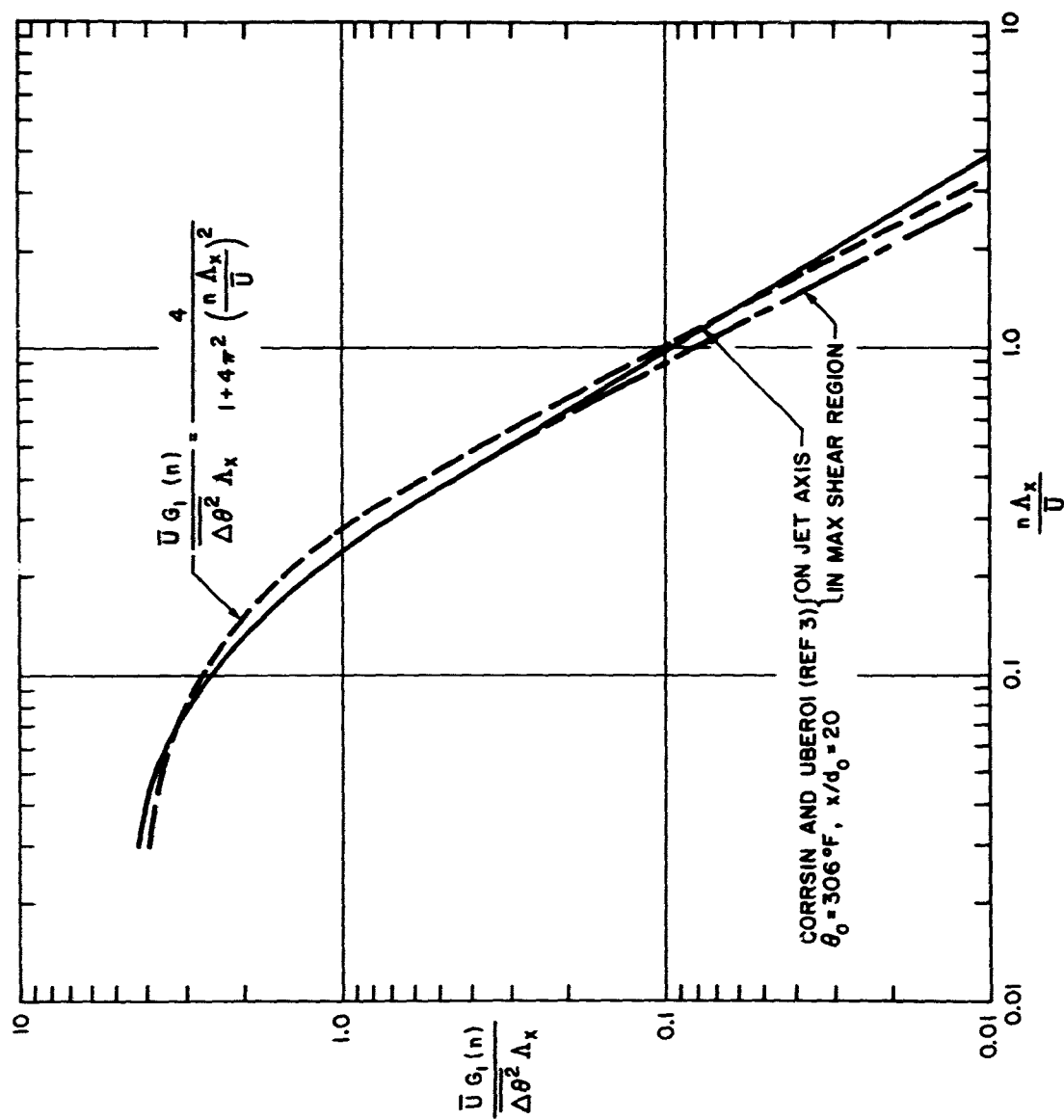
Figure 12. Power spectra of temperature fluctuations

$$\frac{\bar{U}\,G_1\,(n)}{\overline{\Delta\theta^2}\,\Lambda_x} = \frac{4}{1+4\pi^2\left(\frac{n\,\Lambda_x}{U}\right)^2}$$

CORRSIN AND UBEROI (REF 3) $\left\{\begin{array}{l}\text{ON JET AXIS}\\ \text{IN MAX SHEAR REGION}\end{array}\right.$
$\theta_0 = 306°F,\ x/d_0 = 20$

$\dfrac{n\,\Lambda_x}{U}$

$\dfrac{\bar{U}\,G_1\,(n)}{\overline{\Delta\theta^2}\,\Lambda_x}$
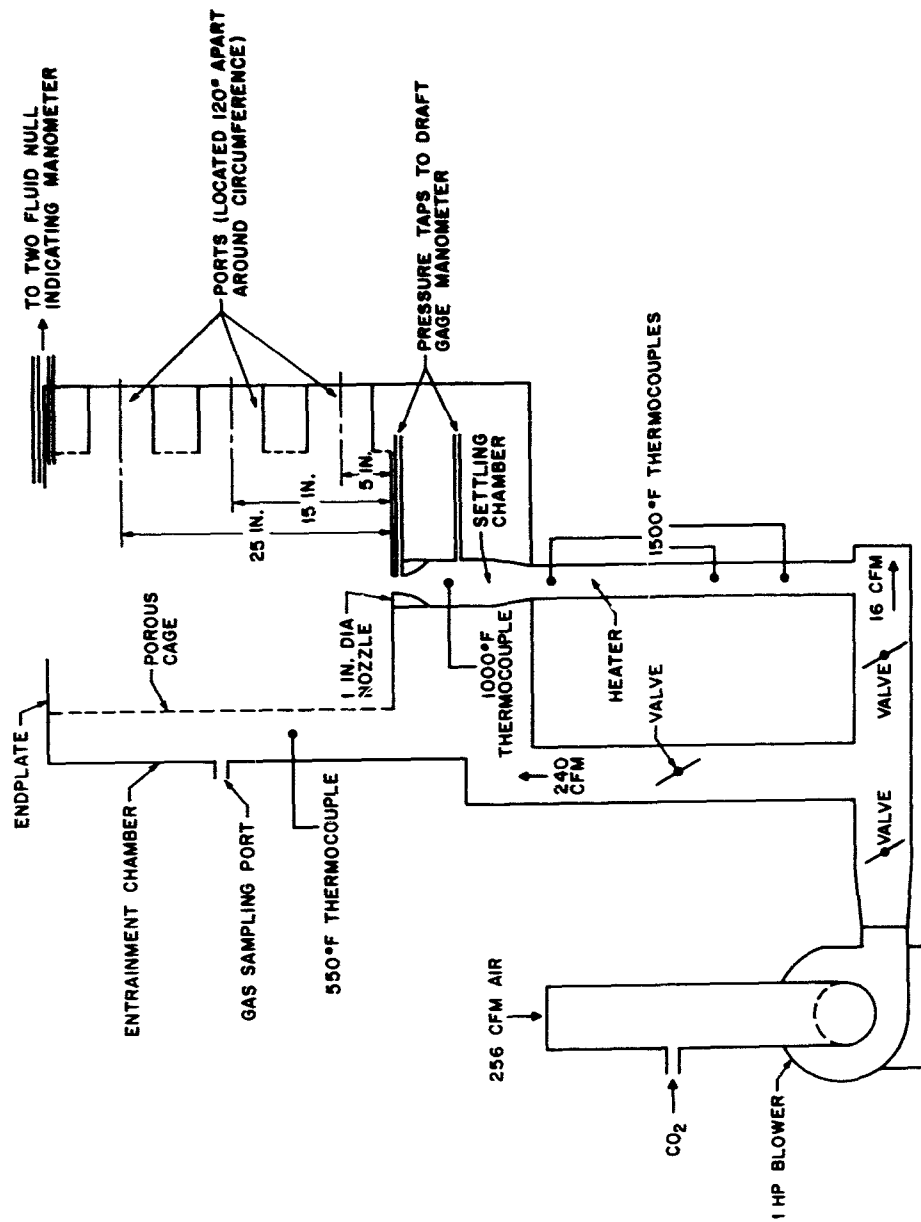
Figure 13. Schematic of subsonic jet setup

37   MC 61-5-R5
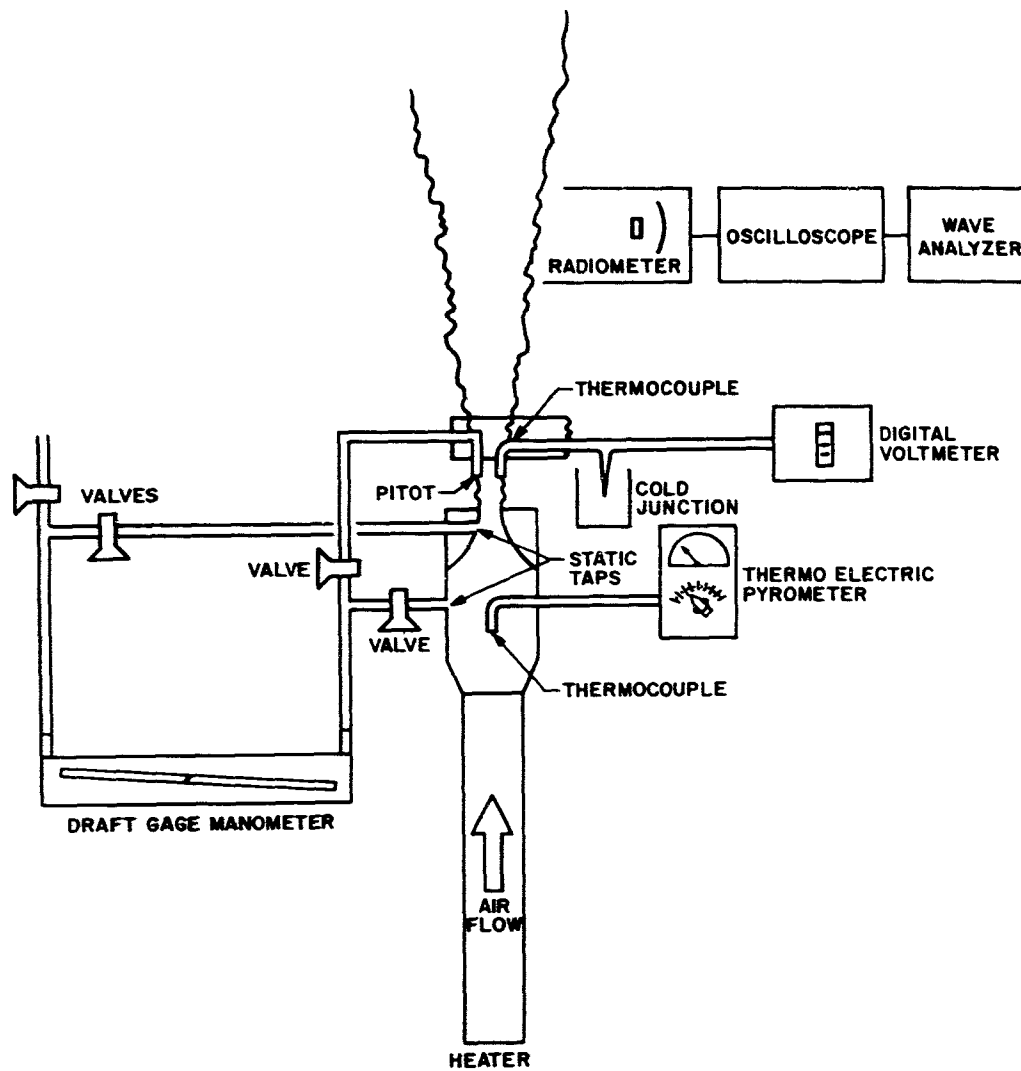
Figure 14. Schematic of hot jet calibration

MC 61-5-R5
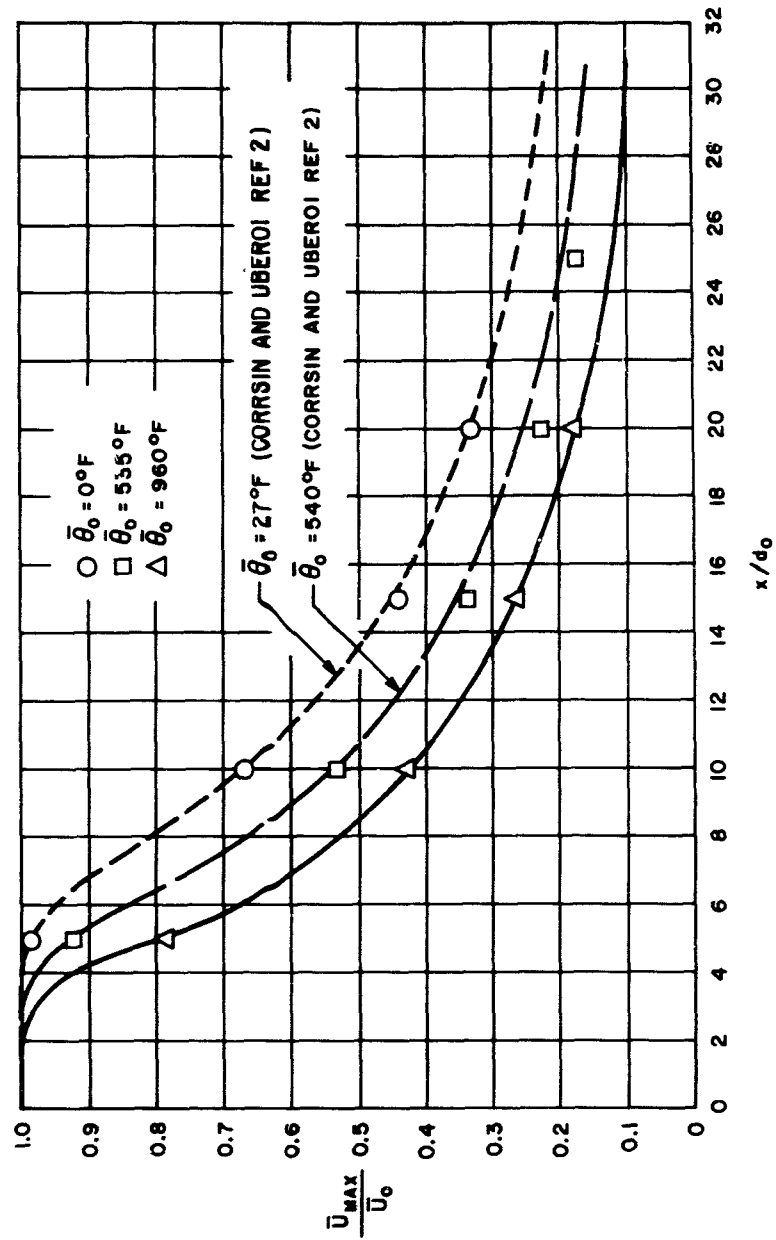
Figure 15. Axial velocity distributions

39
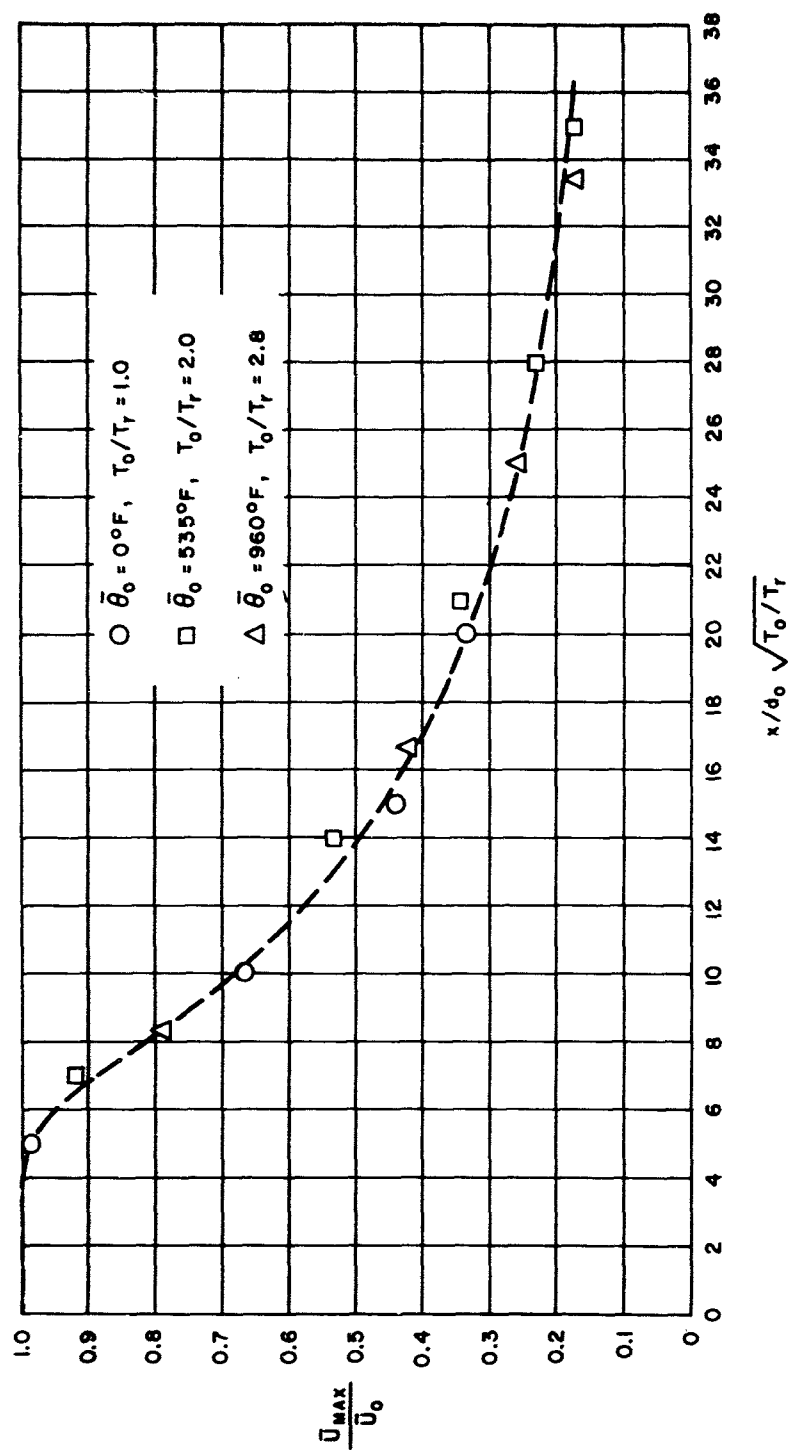
Figure 16. Correlated axial velocity distribution
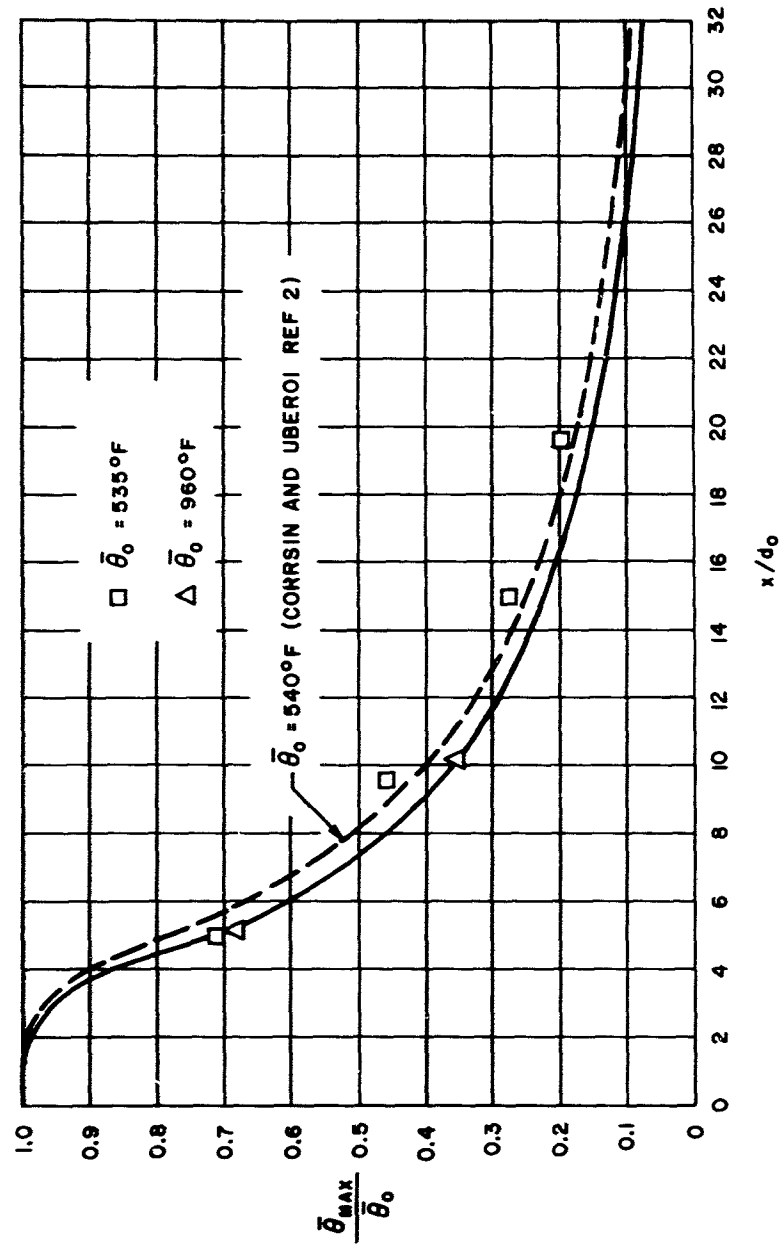
MC 61-5-R5

Figure 17. Axial temperature distributions

41   MC 61-5-R5

Figure 17. Axial temperature distributions

MC 61-5-R5
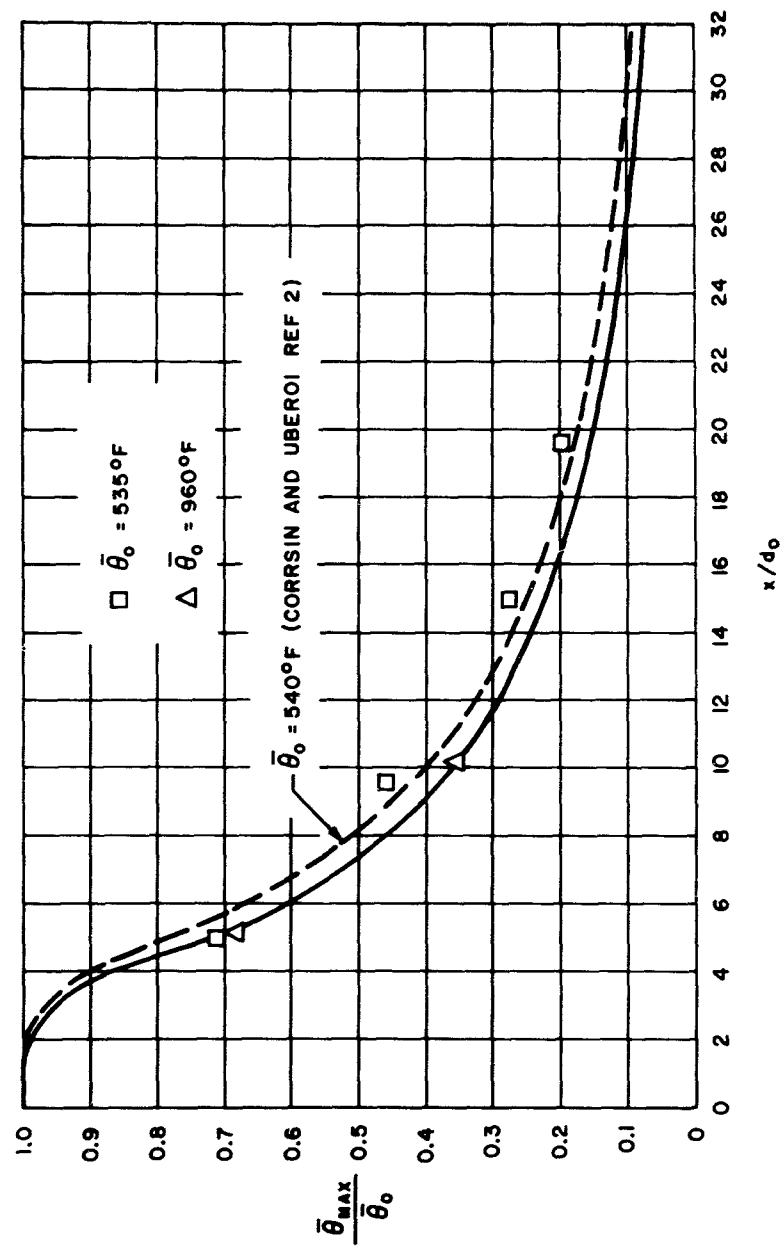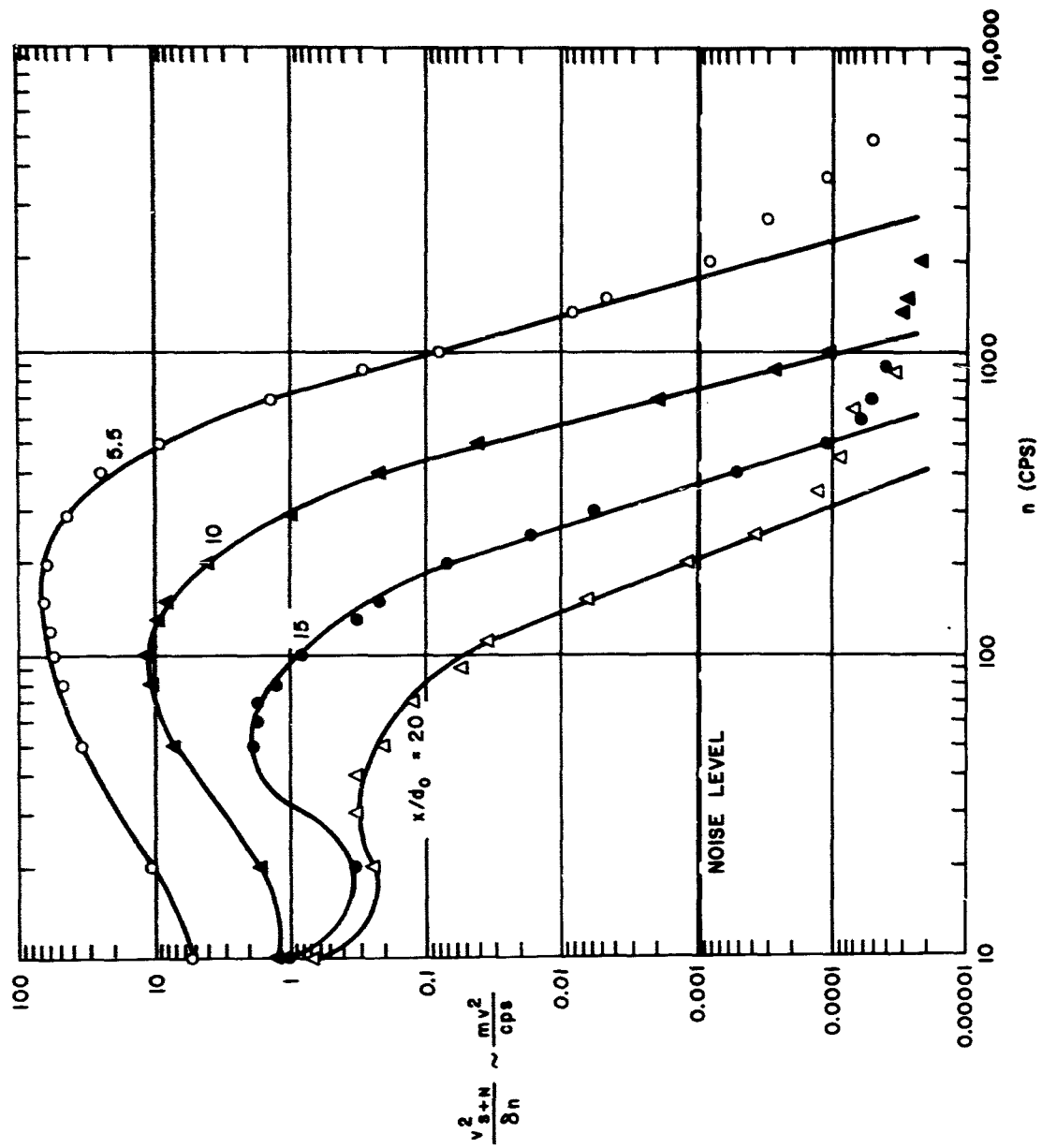
Figure 18. Radiation spectra measured in hot jet.

5.5

10

15

$x/d_o = 20$

NOISE LEVEL

$\frac{v^2_{s+n}}{\delta n} \sim \frac{mv^2}{cps}$

n (CPS)

100

10

1

0.1

0.01

0.001

0.0001

0.00001

0.000001

10

100

1000

10,000

42

MC 61-5-R5
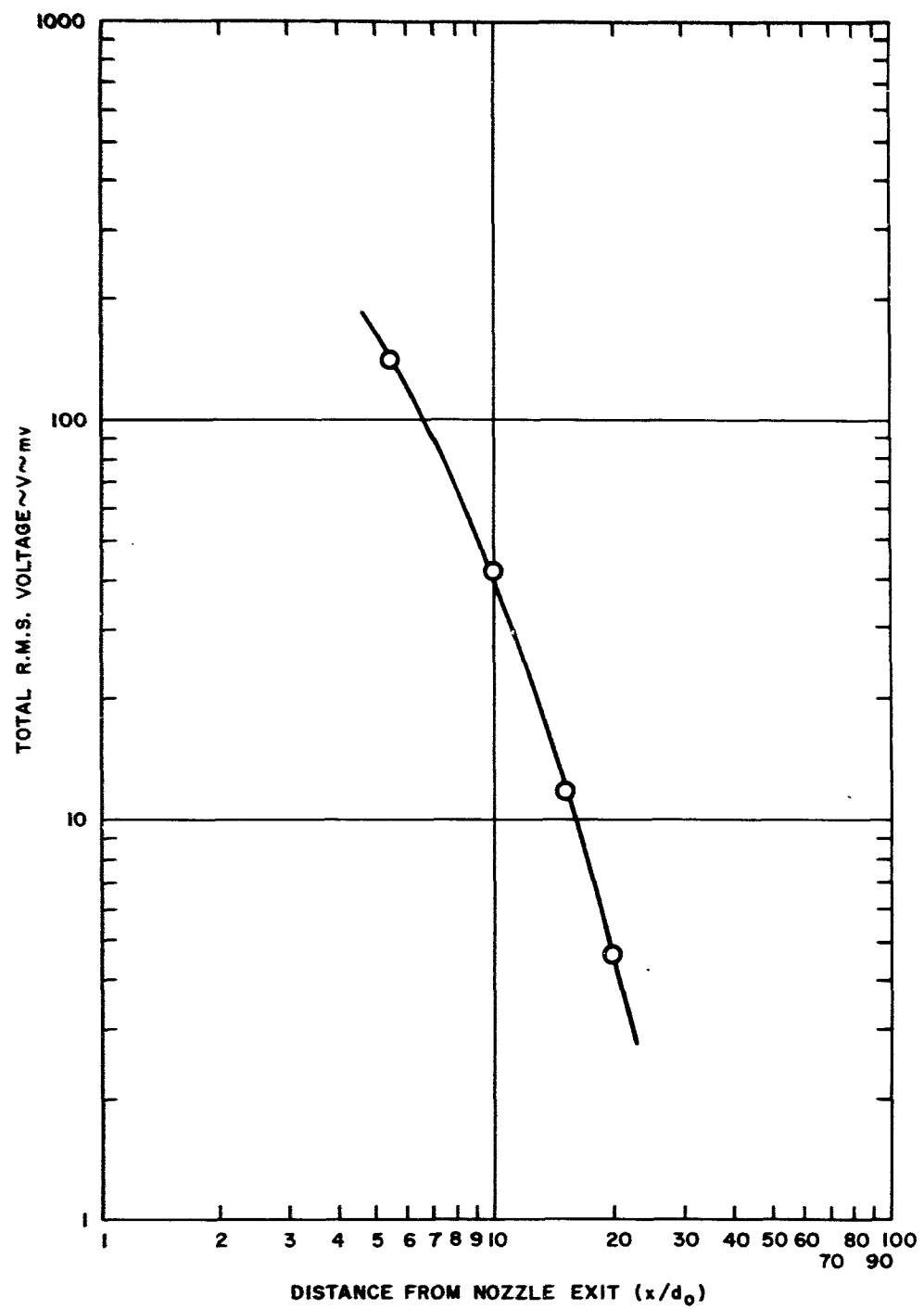
Figure 19.   Total RMS voltage
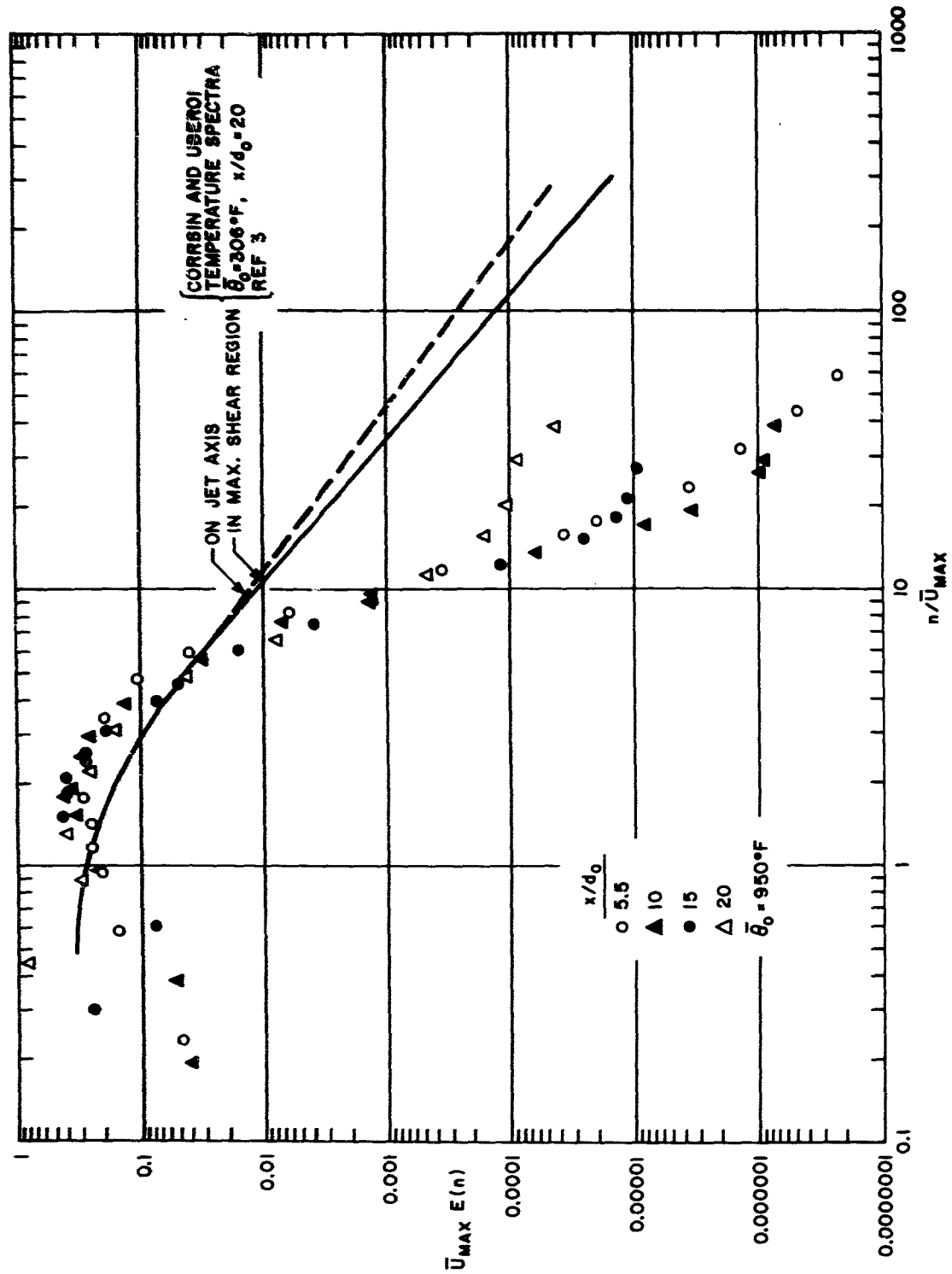
Figure 20. Normalized radiation spectra measured in hot jet

44

MC 61-5-R5
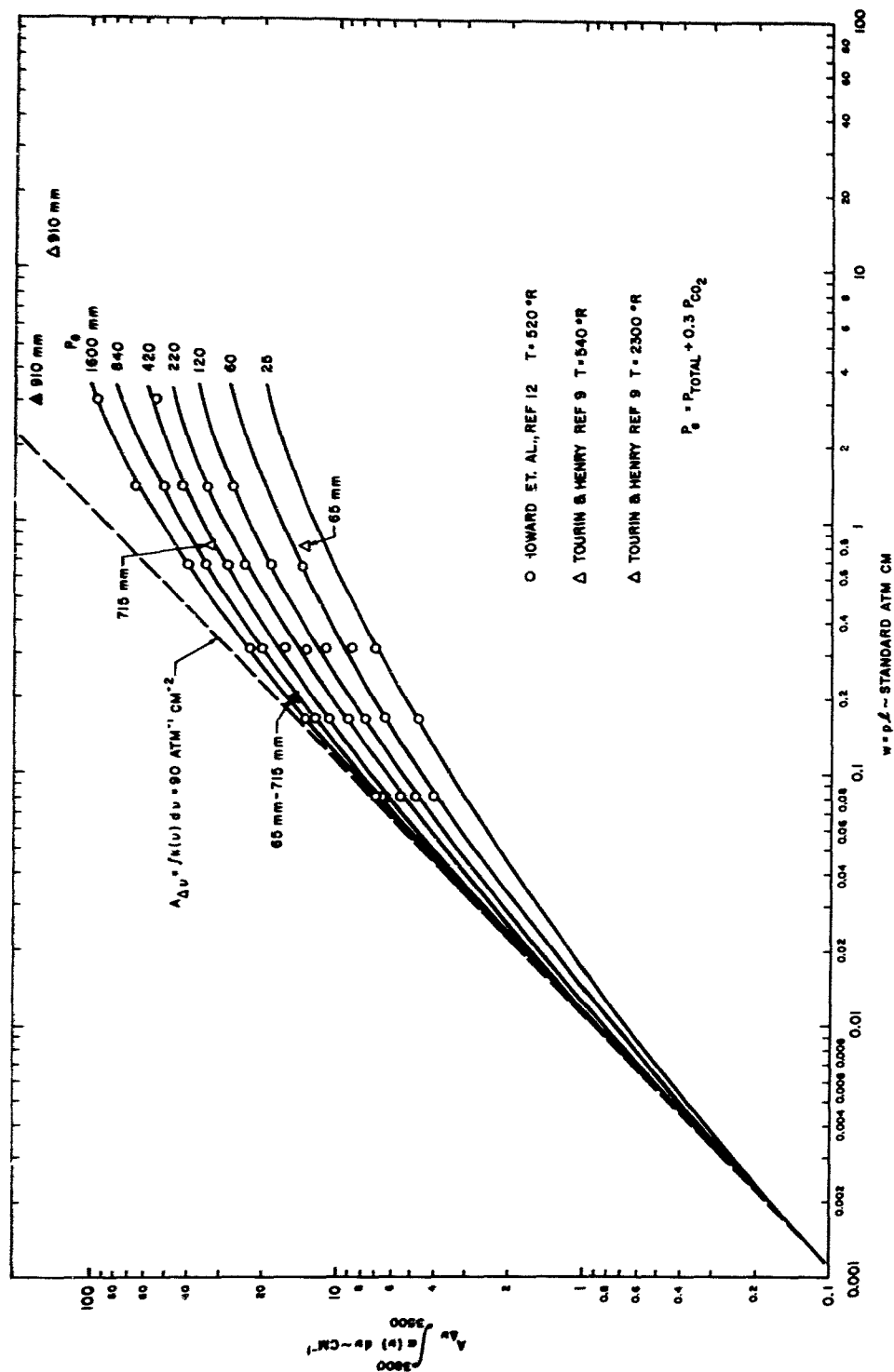
Figure 21. Total absorption vs optical path length for 2.7 μ region of CO_2

45

MC 61-5-R5
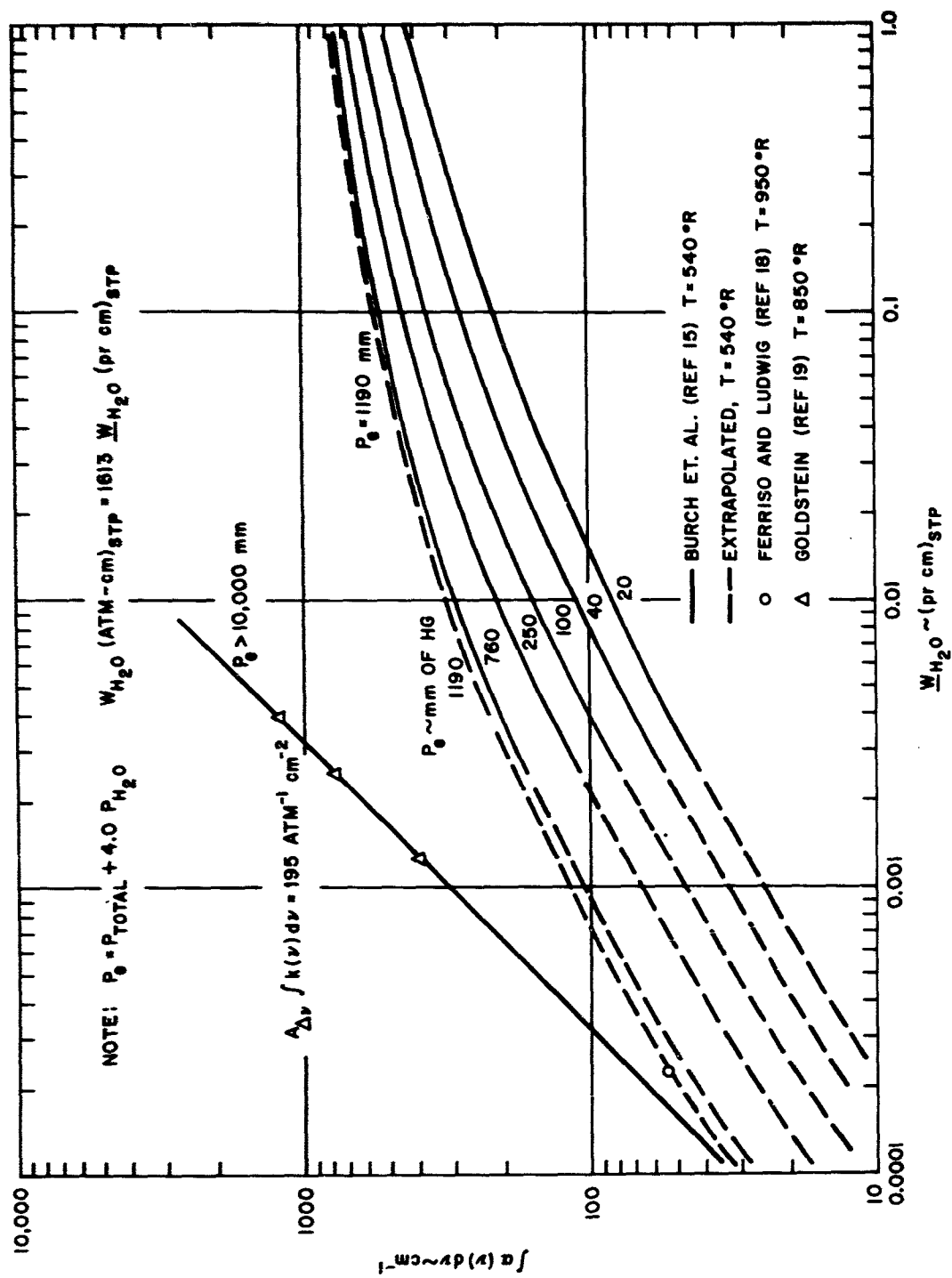
Figure 22. Total absorption vs optical path length for 2.7 μ region of H_2O
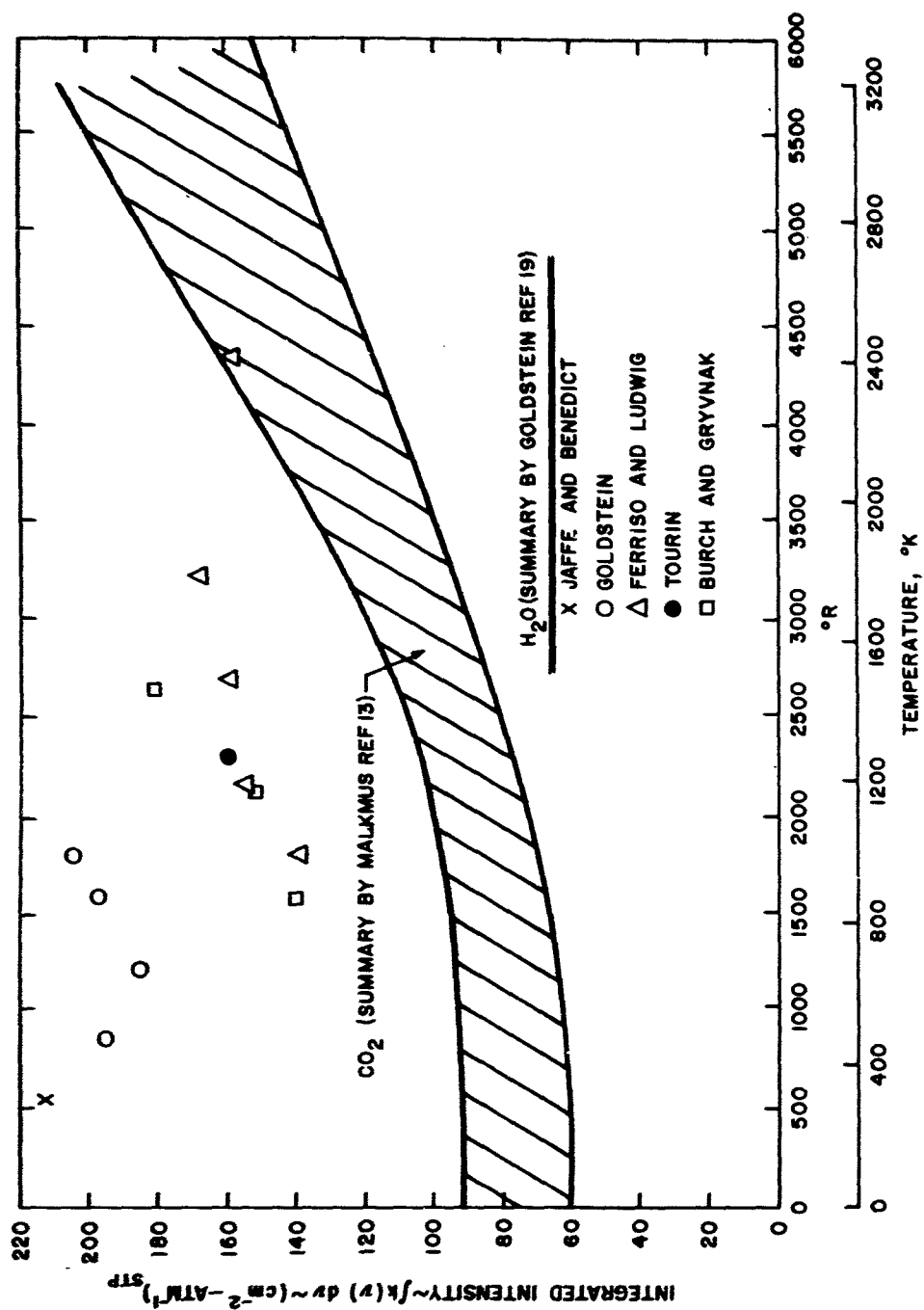
Figure 23. Summary of integrated intensity of 2.7 μ region of CO_2 and H_2O vs temperature

47

DISTRIBUTION LIST

United States Navy

	Attention:
Chief, Bureau of Naval Weapons Department of the Navy Washington 25, D.C.	RMGA-8 (two copies) RM-371 (one copy) RM-372 (one copy) RRRE-3 (one copy)
Director Naval Research Laboratory Washington 25, D.C.	Code 2020 (two copies)
Commanding Officer Naval Ordnance Laboratory, White Oak Silver Spring, Maryland	The Library, Room 1-333 (one copy)
Commanding Officer Naval Missile Center Point Mugu, California	Technical Library (one copy)
Commanding Officer Naval Ordnance Test Station China Lake, California	Technical Library (one copy)
Chief of Naval Research Department of the Navy Washington 25, D.C.	Code 421 (one copy) Code 461 (two copies) Code 463 (one copy) Code 438 (one copy)
Commanding Officer Office of Naval Research Branch Office 495 Summer Street Boston 10, Massachusetts	Mr. Thomas B. Dowd (one copy)
Commanding Officer Office of Naval Research Branch Office Box 39, Navy No. 100, Fleet Post Office New York, New York	LCDR R. W. Adler (one copy)
Commander David Taylor Model Basin Washington, D.C., 20007	Norman Ziegler Aerodynamics Laboratory (three copies)

United States Air Force

Director of Development Planning Headquarters United States Air Force Washington 25, D.C.	(one copy)

MC 61-5-R5

Commander Air Force Office of Scientific Research Washington 25, D. C.	SRGL (one copy)
Commander Air Force Cambridge Research Laboratory L. G. Hanscom Field Bedford, Massachusetts	Library (one copy)
Director of Research Headquarters USAF Washington 25, D. C.	AFRSTA (one copy)
Commander Aeronautical Systems Division Wright-Patterson Air Force Base Dayton, Ohio	WCOSI, Library (one copy) ASRNGE-2 Mr. Wm. P. Kennedy(one copy) WCIRW-5, Reports(one copy)
Commander Rome Air Development Center Griffiss Air Force Base Rome, New York	Research Library RCRES-4C (one copy)
Air University Library United States Air Force Maxwell Air Force Base, Alabama	Mrs. Elizabeth C. Perkins Chief, Document Acquisition Branch (one copy)
Commander Air Force Research and Technology Division Bolling Air Force Base Washington, D. C., 20332	Library (one copy)
Commander Air Force Systems Command Andrews Air Force Base Washington 25, D. C.	Library (one copy)

United States Army

Commanding General United States Army Signal Research and Development Agency Fort Monmouth, New Jersey	SIG-EL RDR (one copy)
Commander Army Missile Command Redstone Arsenal Huntsville, Alabama	ORDDW-MD Air Defense Laboratories (one copy)
Commanding Officer Engineering Research and Development Labs Fort Belvoir, Virginia	(one copy)

MC 61-5-R5

National Aeronautics and Space Administration

Director
National Aeronautics and Space Administration   Division Research Information
1520 H Street, N. W.   (one copy)
Washington 25, D. C.

Others

IRIA University of Michigan
Willow Run Laboratories   Librarian
Ypsilanti, Michigan   (one copy)

Advanced Research Projects Agency
Washington, D. C.   Ralph Zirkind (one copy)

Aerospace Corporation
El Segundo, California   Library (one copy)

Defense Documentation Center
Cameron Station   (twenty copies)
Alexandria, Virginia

50   MC 61-5-R5

MITHRAS, Inc., Cambridge, Massachusetts MC 61-5-R5
NEAR FIELD INFRARED BACKGROUND NOISE SIMULATION
by R. H. Adams, ONR Contract Nonr 3489(00), January 1965

Studies on the near field infrared background noise problem have been directed towards the simulation of the infrared noise emanating from a known turbulent zone. A laboratory tool for simulating the near field noise has been designed, utilizing a simple heated round free subsonic jet as the infrared noise generator. A review of the characteristics of the hot free subsonic jet is presented and the design of the near field infrared background simulator is described. Preliminary measurements of the fluctuations in radiant emittance from the jet have been made with an AC radiometer. The data have been reduced to normalized spectral density curves. The spectral density curves exhibit a more rapid decrease in energy level with increasing frequency than do spectral density curves obtained from hot wire measurements. Finally, a brief literature survey has been made of the infrared properties of CO_2 and H_2O in the 2.7μ region for small optical pathlengths and elevated temperatures. The absorption data presented are especially applicable to laboratory experiments.

1. Near field infrared background noise simulator.
2. Fluctuations in a subsonic jet.
3. CO_2 and H_2O radiation at 2.7μ
I. MITHRAS, Inc. MC 61-5-R5
II. Contract Nonr 3489(00)
III. Adams, R. H.